Space Programs Summary No. 37-22, Volume VI

for the period May 1, 1963 to July 31, 1963

Space Exploration Programs and Space Sciences

JET PROPULSION LABORATORY
CALIFORNIA INSTITUTE OF TECHNOLOGY
PASADENA, CALIFORNIA

August 31, 1963

Contents

THE LUNAR PROGRAM

THE PLANETARY–INTERPLANETARY PROGRAM

THE DEEP SPACE INSTRUMENTATION FACILITY

OPERATIONAL AND TEST FACILITIES

THE LUNAR PROGRAM

I. *Ranger* Project

A. Introduction

The objective of the *Ranger* Project is to exploit present technology in support of the U.S. manned lunar flight program. Fourteen *Ranger* launchings, using *Atlas-Agena B* rockets, are now planned; five of these flights have been made.

Rangers 1 and *2* (Block I) were engineering evaluation flights to test the basic system to be employed in later lunar and planetary vehicles. Several scientific experiments were carried, but on a noninterference basis. The *Ranger 3*, *4*, and *5* (Block II) spacecraft carried a gamma-ray instrument, a radar reflection experiment, a TV camera, and a rough-landing seismometer capsule. All three of these flights failed. As a result, the objectives of future flights have been reviewed, and subsequent design modifications are being accomplished.

The over-all functional and detail designs of the *Ranger* Block III spacecraft (*Rangers 6–9*) are complete. The basis chosen for the new design was that of the former *Ranger 8*, less nonvisual instruments.

B. Design Integration

1. Command Subsystem

The *Ranger* command subsystem is divided into two types of equipment: flight and ground. The manner in which these two portions of the command subsystem are related to each other and to other equipment is indicated in Fig. 1.

Information is conveyed in the Block III command subsystem by use of an 18-bit binary command word. Each bit is 1 sec long. There are two types of commands: the first takes the form of a command that is to be executed by the spacecraft upon receipt of the command (such as begin midcourse maneuver, turn on power for TV subsystem, etc.) and is designated a real-time command; the second type is a transfer of quantitative information from the ground to the spacecraft (such as midcourse velocity increment, terminal maneuver yaw duration, etc.) and is designated a stored command. The command word format and examples of both types of commands are indicated in Fig. 2. The first bit of the

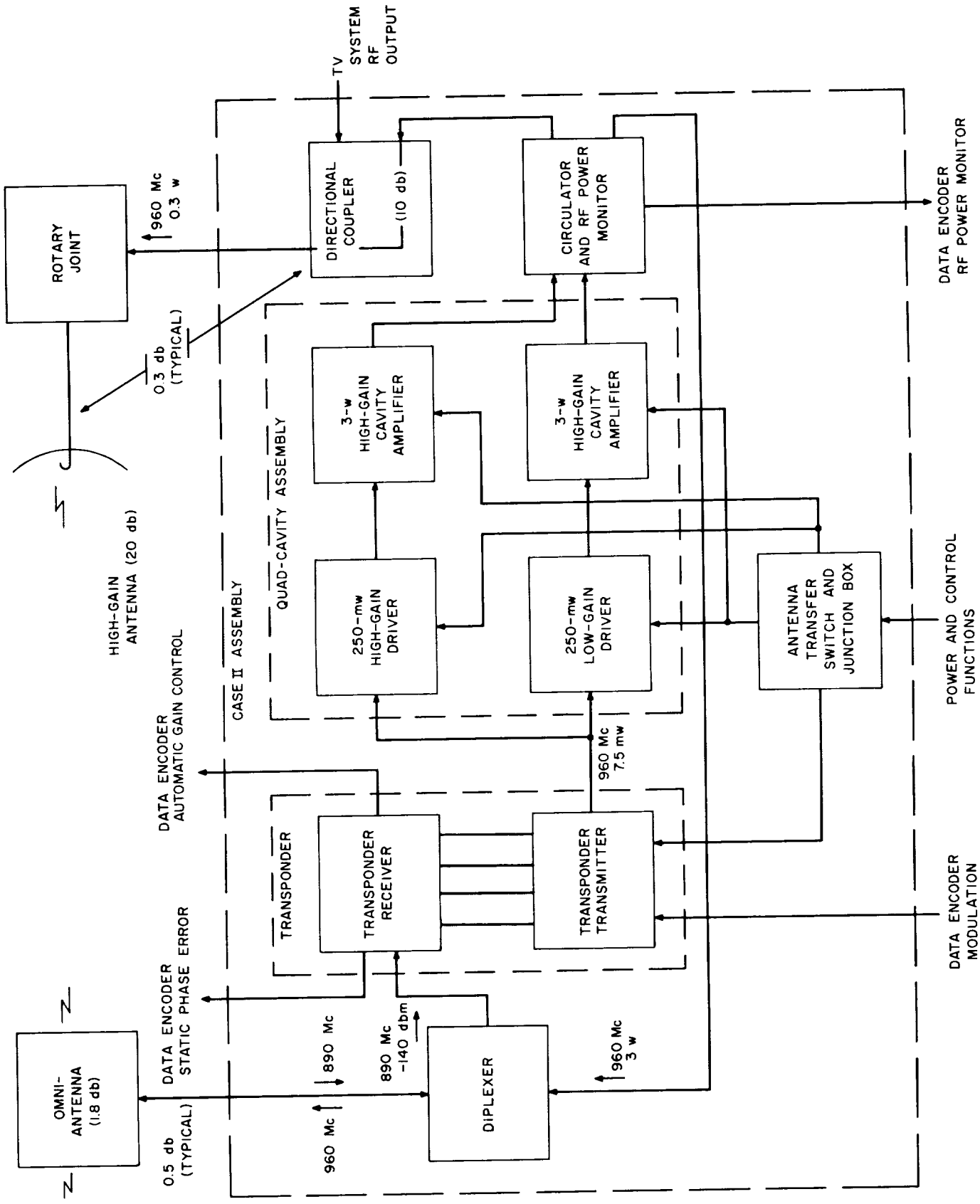

Fig. 3. Mark II L-band communication system

reverse-direction attenuation (20 db) to the cavity amplifiers; this serves to reduce the adverse effects of the high voltage standing wave ratio experienced when the directional antenna is in its stowed position.

d. Antenna transfer switch/junction box assembly. The nomenclature of this subsystem is somewhat misleading since the antennas themselves are not switched. Instead, filament power is switched between the high-gain (or directional) antenna cavity amplifiers and those of the omnidirectional antenna. The antenna transfer switch/junction box also serves as an interconnecting point for wiring between modules and provides direct-access monitoring points during testing at the Spacecraft Assembly Facility.

e. Omnidirectional antenna. The omnidirectional antenna is of the disc-cone type, contained in a truncated cone housing mounted at the apex of the spacecraft frame. It is used for receiving throughout the flight and for transmission from launch until the spacecraft is maneuvered into a position where the high-gain antenna may be employed. An 890/960-Mc *diplexer* permits the dual antenna function.

f. Directional antenna. The JPL telecommunications directional antenna, consisting of a turnstile element backed by a 4-ft parabola, has a forward gain of 18 db. This high-gain antenna is also common to the RCA TV subsystem through a *directional coupler*. Although 10 db are lost by JPL telecommunications through this arrangement, the signal level is more than adequate for lunar missions. Since this antenna must be positioned to face the Earth during flight, it receives its RF energy through a rotary joint in the transmission line.

3. Gas Actuator

The dual gas system criteria have been described briefly in previous issues of the *SPS*. Each half system (i.e., assembly) is made up of one 8-in. vessel, one pneumatic regulator (inlet pressure, 100 to 3500 lb/in.^{2}; outlet pressure, 15 to 1.2 lb/in.^{2}), and six reaction control valves (thrust level, 2 to 6 g). The half system is supplied as a unitized assembly, the majority of which is of welded construction. Also included integral with the assembly is a cable harness which electrically ties in the valves, a high-pressure telemetry transducer, and a telemetry temperature transducer. A ground support fill valve assembly (described in *SPS 37-19*, Vol. VI), which contains a shut-off valve, bacteria filter, and venting check valve, is supplied with each assembly for contamination control. This valve assembly is removed from the gas system prior to flight. Fig. 5 illustrates one gas system assembly installed on the proof-test model.

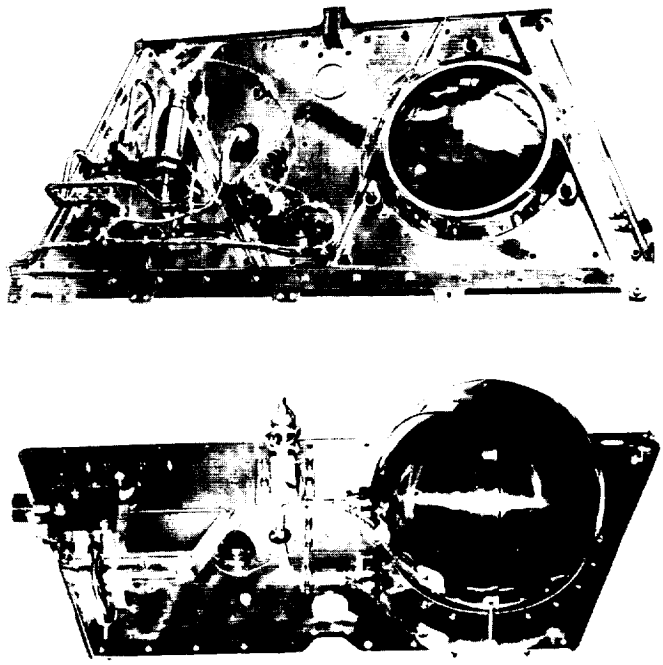

Fig. 5. Block III gas system equipment plate assembly

C. Space Flight Operations

1. Space Flight Operations System (SFOS)

Plans for the checkout of the SFOS are currently being formulated. The tests will (1) verify the compatibility between the spacecraft and the facilities required to support the spacecraft after launch, and (2) develop the operational methods and procedures of the Space Flight Operations Complex (SFOC).

The first category includes the spacecraft operations compatibility tests, the purposes of which are to ensure that (1) the ground-based facilities are compatible with, and can process telemetry and tracking data received from, the spacecraft, and (2) the ground-based facilities can generate commands for transmission to the spacecraft. The objectives of these tests will be accomplished

all real-time analysis capabilities. The PDP-1 computer, which was not available for previous *Ranger* missions, is currently being programmed to receive, process, and display on-line the spacecraft telemetered measurements for the SDAT real-time analysis.

The PDP-1 computer processing consists primarily of data test and checking criteria such as: (1) the determination of the quality of each data sample, (2) a check of the data sample for parity violations and correction of those violations which can be isolated to a discrete level, (3) performance of programmed resync tests on discrete data addresses and resync of those data values misaddressed, (4) conversion of data values of discrete addresses to engineering units, and (5) rearrangement of the data into a more suitable output format. The data will then be routed on-line to the various display equipment of the SDAT (Fig. 6).

The *Ranger 6* data display configuration will provide each subsystem representative with a device displaying only those measurements related to his subsystem. The data will be displayed in tabular form and will be computer processed, enabling subsystem analysis to be performed more rapidly and efficiently.

b. DSIF. New telemetry equipment, composed of Beckman decommutators driving a modified *Mariner*-type telemetry encoder, formats data for subsequent teletype transmission so that all low-rate telemetry measurements and selected high-rate measurements are capable of being available to the SDAT in essentially real time.

The old telemetry equipment configuration used for the *Ranger* Block II missions will be kept intact at the stations to provide backup support to the new equipment if necessary.

c. Spacecraft design characteristics. The spacecraft command logic has been modified such that the Real Time Command (RTC) 1 (*roll-override*) now also serves as a backup command for turning on the Earth sensor power, thus enabling the SDAT to recommend additional corrective measures in the event of discrete failures in this area.

A new command, RTC-8, has been added to the Block III series. This command gives the added capability of disabling the midcourse motor from firing in the event the spacecraft were to go into an incorrect or continuous roll and/or pitch turn during the command maneuver.

The number of preset hinge angle settings for the directional high-gain antenna has been increased from four to eight. This modification will give additional angle selectability in the event difficulties are encountered at the Earth acquisition or reacquisition sequences.

Two central computer and sequencer programmed events, *open solar panel* and *acquire Sun*, were set to occur 12 min later on the Block III series to ensure that these events would occur in the view of a tracking station and could be monitored and analyzed by the SDAT in real time.

The spacecraft telemetry system has been modified to switch to Telemetry Mode II (midcourse maneuver) at the end of the pitch turn, enabling measurements to be recovered during both roll and pitch turns and enabling the SDAT to perform more real-time analysis of the commanded maneuvers.

D. Testing Operations

1. Antennas and RF Components

High-power components of the spacecraft RF subsystem have been subject to a breakdown phenomenon in high vacuum called multipacting. The RF power handling capability testing and evaluation of the modified components required the design and construction of a test setup with a 120-w RF source, a recording system, and a means of reducing the required time of testing to a reasonable duration.

A cavity amplifier chain was constructed and tested. The recording system, using a four-channel Sanborn recorder, preamplifier, and HP 413A power meters, is capable of measuring and recording forward, back, and load powers.

A ready source of free electrons is required to avoid a long wait before a breakdown occurs. A radioactive source of cobalt 60 has been obtained and is being utilized to determine the optimum level of radiation. Initial tests indicate that a 1-Mc source located 7 in. from a Type N connector will induce a breakdown in a few minutes, as compared to as long as several hours without the use of a radioactive source.

During the vibration testing, a crack occurred in one of the glass filters used to cover each of the 4,896 cells contained on the solar panel. During the last 36-sec 96-rms-noise burst of the high-frequency pitch test, a wire on one of the zener diodes associated with Section 3 broke loose from its solder connections.

On April 20, the vacuum-temperature and thermal shock test was initiated in the JPL 6-ft vacuum chamber. During this test, an operations error caused a failure in one of the zener diodes. The post-vacuum-temperature electrical performance test of TA 1 at Table Mountain revealed that two cells in Section 3 had opened—one on the negative side and one on the positive side. There was no apparent degradation in the extrapolated maximum power output in Earth–space due to this environmental test.

On April 29, TA 1 was subjected to a temperature-humidity environment in the JPL humidity chamber (Fig. 9). There was no apparent damage to the cells during this environmental test.

Because of the failures which occurred in panel TA 1, it has been completely reworked and will go through TA testing again. In addition to TA 1, a second TA panel (TA 2) was built using low-efficiency solar cells. Panel TA 2 is intended mainly for use with TA 1 in tests to be conducted on the structural-test-model spacecraft. However, both panels will be subjected to complete TA testing after these tests.

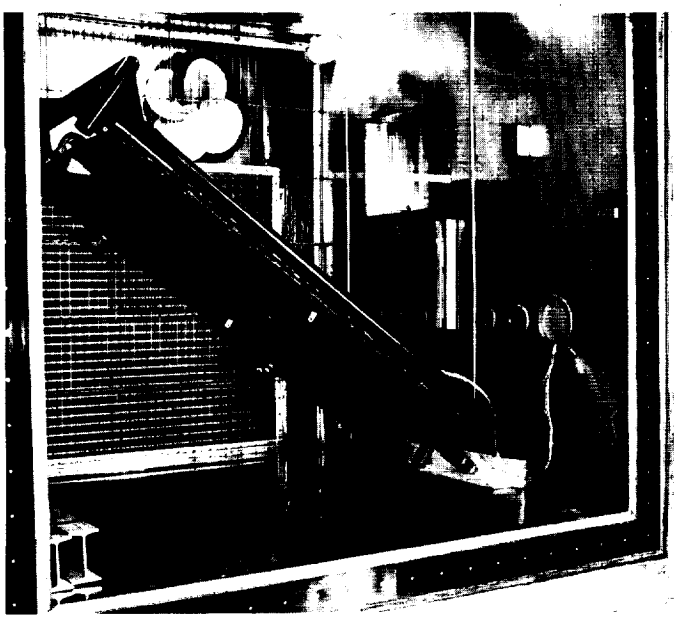

Fig. 9. Humidity chamber

4. *Life Test Vehicle (LTV)*

Testing of the LTV was completed June 8, 1963. The purpose of the program was to determine spacecraft performance in a long-term simulated space environment. The LTV consisted of the former *Ranger 6* spacecraft bus, cables, and electronics, with minor exceptions. The TV subsystem used was the former Flight Model 2.

Upon completion of all tests, the LTV was returned to the Spacecraft Assembly Facility and disassembled. The hardware was bench-tested to determine if any degradation resulted from the 33 days spent in vacuum.

With the exception of a power converter failure in one of the tests, all mission tests were partially successful in that, had the spacecraft actually been launched, good data, including TV pictures, would have been obtained. The difficulties encountered with the TV subsystem were, on the whole, in known problem areas. Many of these problem areas have been eliminated through redesign for Block III, and the remainder are under investigation.

5. *Proof-Test Model (PTM)*

On May 29 at the Spacecraft Assembly Facility, the power turn-on test was performed. The spacecraft power subsystem (Block III design) operated successfully, with each subsystem simulated by dummy loading of the booster regulator output. Each subsequent subsystem was subjected to an initial power turn-on test.

Mechanical operations performed during the subsystem test phase included:

(1) Checkout of hardware interface compatibilities for the PTM and *Ranger 6* flight spacecraft.

(2) Installation and testing of the backup command timer.

(3) Pressurization, calibration, and operation of the attitude-control dual gas system.

(4) Mating of the TV subsystem with the spacecraft bus.

By the end of the test phase period, all spacecraft subsystems were tested in at least their electrical equivalent form.

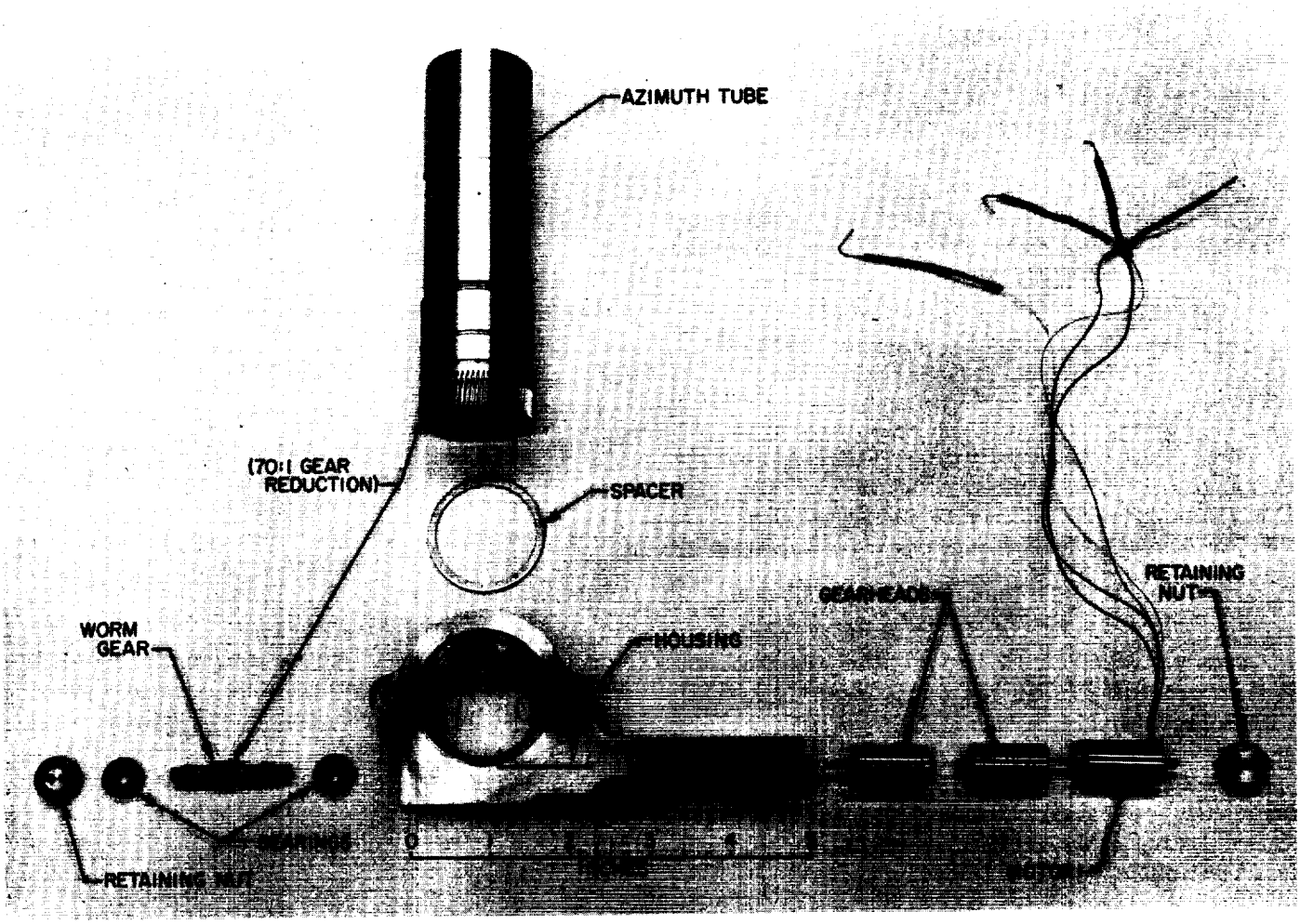

Fig. 10. Prototype of azimuth drive mechanism

The motor/gearhead combination was subjected to a lateral impact in excess of 3000 *g*. Functional tests performed prior to and following impact indicated no deterioration of performance. Additional impact tests of these components are being scheduled.

c. Extension mechanism. Development test hardware and associated fixtures have been fabricated and assembled. Preliminary tests were conducted on the engineering developmental extension system. The setup provides for evaluation of the effect of control orifice size and capsule gas volume. Extension velocity, extension pressure, and top-tube shock are also instrumented to allow for performance evaluation. Preliminary results indicate that the range in extension velocity of 2 to 11 ft/sec determined from the functional model tests is also valid for the full-size system. Tests are continuing to establish the proper control orifice diameter and the effect of variation in available gas volume.

d. Impact limiter. Capability to produce higher reaction loads and thereby increase deceleration levels has been achieved by incorporation of a new limiter designated Mark VIII-B. The Mark VIII-B limiter consists of a Mark VIII balsa wood limiter stiffened with four 1-in. D nylon rods to give increased load stroke characteristics. The estimated *g*-level increase resulting from this modification is 700 *g*. To withstand the higher loadings, the Hyge sled has been reinforced with bonded shear skins. Fig. 11 shows the modified sled contacting the Mark VIII-B limiter.

e. Signal and synchronization electronics. A breadboard has been tested and meets all requirements of the design specifications. In the synchronous demodulation mode, 45-db dynamic range has been achieved with good linearity. The demodulator is fail-safe against loss of the reference signal by functioning as an envelope detector.

The design concept for the split-system configuration was finalized during this reporting period. Modification of existing assemblies and fabrication of new assemblies have been initiated for the Block III flight models (FMs), and environmental acceptance tests of the assemblies for the Block III-1 FM are being completed. Work on Block III in the thermal control area was concentrated on the preparation of a Block III-1 FM thermal shield and testing of the temperature sensors.

The performance of the split-system configuration has been tested, and compatibility of the dual-channel TV subsystem is assured. Test results indicate that the concept of two essentially independently operative camera and communication chains, together with the revised fusing philosophy, have increased the probability of mission success by decreasing the subassembly-failure vulnerability of the entire spacecraft. Previous failures which would have been "catastrophic" are now relegated to a non-optimum mission classification. The failure of one of the channels now will only reduce the information capability of the TV subsystem.

Conversion of F-scan cameras to fast-erase (15 kc) was completed, as well as camera calibration and communications checkout and alignment. The lightweight battery mounting, the camera electronics thermal shield, the camera boresight range, and the collimator bracket to accommodate a new 25-mm, *f*/0.95 lens were designed. All design modifications for the split-system configuration are now complete with respect to the ground support equipment.

With the exception of a power control unit and an electronic clock, the Block III proof-test model (PTM) was assembled and progressed satisfactorily through the planned test program. During a series of thermal-vacuum tests, satisfactory operation of the PTM in a simulated space environment was demonstrated. As a result of the tests, a modification was made in the thermal shield. This change will cover the area where electronic equipment was exposed because of the enlarged camera field-of-view hole. The modification will be a thermal insulator; therefore, the outside can be painted black to avoid reflections to the camera lenses. The insulator will be made of six layers of aluminized Mylar, sewed together and zippered to an outer plate 0.020 in. thick. The outer plate will be painted black and secured in position. Structural modifications to the PTM split-system configuration were proven adequate by the successful completion of the PTM vibration test at acceptance-test levels.

The thermal control model was reworked to the Block III configuration. The second in a series of solar simulation tests at the JPL solar simulation facility was completed during this reporting period. This test used the thermal-control-model bus, and fin extensions (solar shields) were attached to the fins of the TV subsystem to eliminate illumination of the thermal shield. The data obtained show that the average vehicle temperature expected during flight is 17°C.

Simulated mission testing of the life test model (formerly, FM 2) continued, and satisfactory results were obtained.

Table 1. *Surveyor* scientific payload

Experiment	Weight, lb	Investigator; co-experimenters
TV (2 horizontal cameras)	37.2	E. M. Shoemaker (NASA/USGS); G. P. Kuiper and E. Whitaker (University of Arizona)
Micrometeorite ejecta	8.5	W. M. Alexander (GSFC); O. E. Berg, L. Secretan, and C. W. McCracken (GSFC)
Seismometer (single-axis)	10.0	G. H. Sutton (Lamont Geological Observatory); M. Ewing (Lamont Geological Observatory) and F. Press (CIT)
Alpha scattering (instrument deployed to lunar surface)	10.5	A. Turkevich (University of Chicago); J. Patterson (Argonne National Laboratory) and E. Franzgrote (JPL)
Surface sampler (soil-properties measuring device)	11.4	R. F. Scott (CIT); R. M. Haythornthwaite (University of Michigan) and R. A. Liston (U.S. Army Ordnance Land Locomotion Laboratory)
Touchdown dynamics	4.2	S. A. Batterson (LRC)

B. Spacecraft Development

A very recent redefinition of the scientific payload (Table 1) by the Space Sciences Steering Committee of the NASA Office of Space Sciences has led to the initiation of new payload integration and mechanization activities by Hughes, particularly with respect to deployment of the seismometer and alpha-particle instrument to the lunar surface and the expansion of surface-sampler instrumentation to fulfill its revised role.

The match-mate test series conducted at Hughes with General Dynamics/Astronautics *Centaur* forward-bulkhead mockup, nose fairing, and ground handling hardware, using the engineering mockup and prototype spacecraft (*SPS 37-21*, Vol. VI, pp. 26–28), were satisfactorily concluded during this period. Results of the RF isolation tests using the prototype spacecraft inside the nose fairing with a thin external aluminum blanket has assured RF protection of the individual encapsulated spacecraft from RF interference or interaction with other spacecraft during preflight operations.

Another *Centaur–Surveyor* interface test conducted at this time was the spacecraft separation test. This test provided data on separation dynamics, utilizing the landing-dynamics drop-test spacecraft, a *Centaur* forward-bulkhead mockup, and prototype separation hardware, with an air-bearing suspension fixture at General Dynamics/Astronautics. The test setup is shown in Fig. 2.

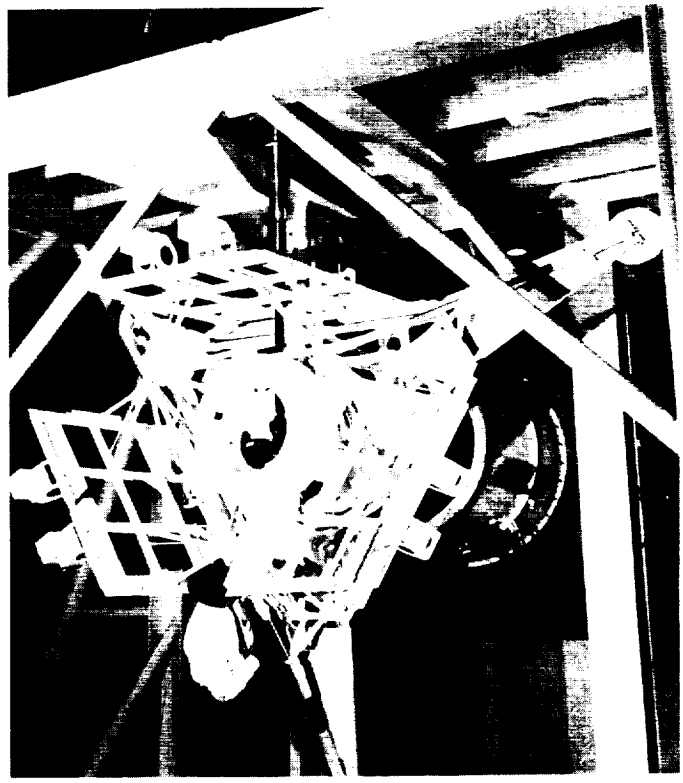

Fig. 2. *Centaur–Surveyor* separation test

The redesign of the original contractor's vernier engine, which resulted in the installation of new throttle valves, is complete; two sets of engines have been delivered. Static tests with the descent-dynamics test spacecraft show promise, and tether tests have resumed. The preliminary design and feasibility-demonstration phase of

III. *Mariner* Project

A. Introduction

The primary purpose of the *Mariner* Mars 1964 mission is to permit a biology-oriented scientific investigation of the planet Mars during the 1964 opportunity. Secondary purposes in order of priority are: (1) to make interplanetary scientific investigations in the region between the Earth and Mars orbits, (2) to develop additional experience in the design of spacecraft capable of conducting specific interplanetary missions, and (3) to provide experience and knowledge which will permit continued development of attitude stabilized spacecraft of the more advanced *Mariner* and *Voyager* types. The *Mariner* Mars spacecraft will be injected into Mars planetary transfer orbit by the *Atlas D* spacebooster/*Agena D* launch vehicle. Two identical spacecraft will be launched during this planetary opportunity.

The *Mariner* Mars 1964 spacecraft design is progressing. Weight continues to be a source of concern. There is a tendency toward a gradual weight increase as the design, and in some instances the hardware, become better known. A continuous accounting of estimated weights and a list of potential design changes are being maintained in case the spacecraft weight remains above the acceptable 570-lb limit when the hardware is assembled.

Because of budgetary considerations, some reduction in project requirements was made. A set of spares for the proof test model, one flight spacecraft, one set of system test complex, and one set of launch complex equipment were dropped. This resulted in foregoing the plans to attempt a third launch during the launch period.

The design evaluation vehicle tests on a *Mariner* Venus 1962 spacecraft have been completed. The associated system test complex will be converted to the *Mariner* Mars 1964 Project where applicable and the spacecraft will be made available for display.

B. Spacecraft Mission Simulation

A digital computer program which will simulate spacecraft missions is being developed for the IBM 7094 computer.

D. Mariner Mars 1964 Spacecraft Design

1. Booster Interface

The *Mariner* Mars 1964 spacecraft/*Agena* interface will include a lanyard-release Cole umbilical connector that is pulled at lift off, and a small 15-pin in-flight disconnect connector. A shear tie will be incorporated on the adapter to react spacecraft torsional loads.

A new lightweight diaphragm will be attached to the aft end of the spacecraft adapter and supported, during flight, on the *Agena* forward section. The diaphragm will provide clearance for the spacecraft planetary science experiment.

2. Mechanisms

a. Planetary science scan mount. The *Mariner* Mars 1964 planetary science payload has been redefined to such an extent that much of the original structural design philosophy has been altered. The present payload consists of the original TV plus the addition of an ultraviolet photometer and narrow-angle Mars acquisition sensor. The over-all effect of this instrument substitution is a significant decrease in weight and improved temperature compatibility.

As a result of the planetary science payload change, the scan platform and cover have been redesigned. The new science bracketry is a one-piece machining riveted to the end of the cantilevered tube, thus providing an integral support for all science packages with good structural stiffness and instrument alignment. The requirement for instrument Sun shades and on-pad checkouts resulted in the design of a removable cover which attaches to the science support bracket and covers the optics of each instrument through midcourse maneuver. The cover consists of a lightweight aluminum honeycomb plate mounted on spring loaded hinges and fitted with the necessary shields for each instrument. The proposed method of cover release is a solenoid actuated latch operated by the squib firing assembly.

b. Scan actuator. Two significant changes to the *Mariner* Mars 1964 scan actuator design have been initiated. To insure scan reversing reliability, an additional pair of limit switches was incorporated as a backup to the original ±90-deg scan limit switches. Also, the original scan drive motor gearhead has been replaced with one made to rigid quality control procedures.

c. Solar pressure vane. The structural portions of the *Mariner* Mars 1964 solar pressure control system are the solar pressure vane, latching mechanism, and deployment mechanism.

As a result of early failure mode analysis, a simpler and more reliable approach has been taken towards the solar pressure attitude stabilization vanes and their stowage and erection system. The vane will be composed of 7 ft^2 of aluminized mylar sheet stretched over a framework of four aluminum tubes (Fig. 1). Each vane is stowed in a furled position against the back of a solar panel during boost. As the panels deploy, the lanyard latch releases the vane, and the deployment mechanism unfolds the vane to its flight position.

Temperature studies of the solar vane and available data indicate that during cruise and midcourse maneuver the aluminized surface on the top side and the mylar lower surface would give temperatures well within the limits of mylar. Current information indicates that the mylar will not be detrimentally affected during the 1- or 2-hr period of midcourse maneuver when the uncoated side may be Sun-oriented.

d. Solar panel actuation system. The redesigned solar panel actuation system consists of eight leaf springs attached to the base of the solar panel beam and a central rotary hydraulic retarder linked by cables to each solar panel.

The retarder is designed to allow the four panels to open simultaneously in approximately 45 sec. The retarder assembly is a hydraulic vane torque motor which develops resistance to motion by forcing fluid from one side of a vane to the other through a tapered orifice and needle. Alcohol is used as the working fluid. If a leak develops after deployment, the alcohol will not adversely affect the optical lenses or temperature control surfaces.

e. Structural dampers. The boost phase dampers for the solar panels and the omni-antenna mast will consist of two concentric, close fitting magnesium tubes with silicone grease held in place between the two tubes by a combination O-ring, teflon slipper seal.

The cruise phase damper for the solar panels is a conventional piston and cylinder hydraulic damper with a centering spring positioned inside the damper. Silicone oil is used as the fluid and a sealing system is used to give maximum protection against leakage.

f. Solar vane actuator. The solar vane actuator will utilize the thermomechanical and electromechanical portions in series. The electromechanical portion will position the thermomechanical portion and a solar vane in order to balance solar pressure bias torques. The solar vanes will cause the center of solar torques to coincide with the center of spacecraft mass maintaining the spacecraft attitude with respect to the Sun. The thermomechanical portion acts as a positive feedback device, damping out the natural oscillations of the spacecraft.

Detail design of the solar vane actuator has been completed (Fig. 2). The actuator is a low power, light weight step-motor, gear train, driven by a ring amplifier employing SCR's for switches. The motor gear train positions the thermal actuator and the solar vane in 0.01-deg increments. The action of the motor gear train is inhibited beyond 20 deg either side of the zero position by a switch assembly which prevents incoming commands from driving the actuator in the direction of the limit. Commands which cause the actuator to retreat from the limit are not affected. A potentiometer has been included which will indicate position of the solar vane when interrogated by the telemetry system.

Weight of the complete actuator, including motor, gear train, electronics, Sun valve, bimetal strip, and potentiometer-switch assembly, will be 8 oz. The motor, gear train, and potentiometer-switch assembly will be sealed with O-rings and carry atmosphere throughout its life.

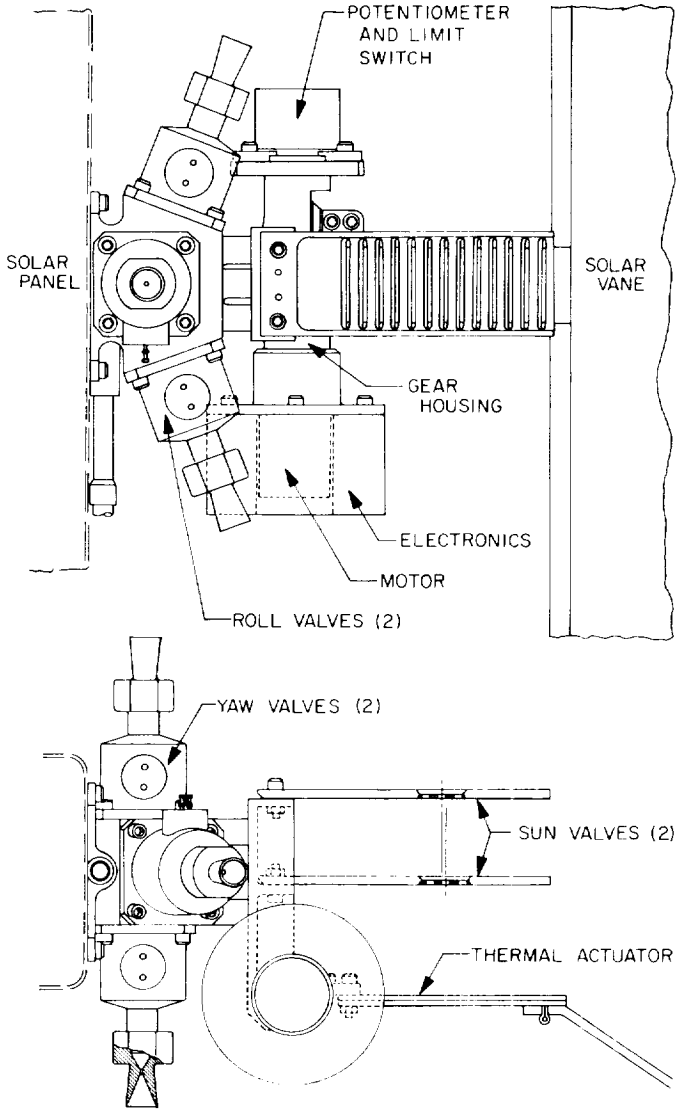

Fig. 2. Solar vane actuator and gas valves

3. Gyro Control Assembly

Design and fabrication of the *Mariner* Mars 1964 gyro control assembly (GCA) has now proceeded to the point that a prototype unit has been finished and brought to the servo test phase (Fig. 3).

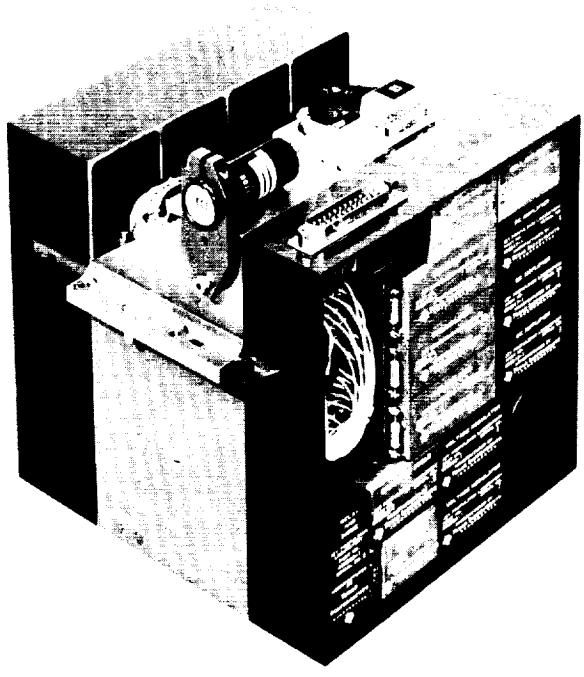

Fig. 3. Prototype gyro control assembly

The GCA consists of three major subassemblies attached mechanically, electrically mated, and calibrated. The units are:

(1) The electronic package which contains all power supplies, rebalance amplifiers, the precision current generator, and other miscellaneous electronics.

(2) The gyro package which contains the three Kearfott C70-2565 gyros.

(3) The integrating capacitor bank which contains twelve special tantalum capacitors, each of 1020 μf, used to store the gyro gimbal motion.

Total weight of the three mated subassemblies is 11.2 lb. Power consumption is on the order of 16 w.

In the servo test phase each gyro in turn is operated in the second mode (commanded turn). The entire assembly is placed on a precision turntable (J. W. Fecker Co.) and is commanded in the same manner as in flight. The table follows the gimbal in the same manner as the spacecraft by means of a very tight servo loop. The turning rate is accurately measured by means of a microgon position readout (3 arc sec accuracy) and a precision digital counter, printer unit. Rates of turn are measured for three ranges of gyro temperatures and for different directions of rotation and different gyro output axis orientations. From this data the gyro torquer scale factor, gyro fixed torques, and mass unbalance are obtained as well as the actual command turn rate. A set of graphs for the performance of the prototype package is shown in Figs. 4 and 5.

4. Power Subsystem

a. Electrical conversion equipment. The completed breadboard model of the 400-cps single-phase power amplifier has been partially revised. Output requirements will be as follows: The space science subsystem will receive 28.0 v rms, ±5%, 400-cps squarewave, and the video tape recorder will receive 32.6 v rms, ±5%, 400-cps squarewave. This change should reduce the weight of the subassembly by about 1.5 lb. Also, the efficiency should increase to above 83% (under full load conditions).

The complete breadboard model of the 400-cps three-phase power amplifier has been modified to provide increased voltage drive to the power transistors. This allows a greater degree of freedom in transistor selection, thereby eliminating the need for using only the high beta units.

b. Solar panels. Using results of the recent *Ranger* Block III type approval solar panel assembly, the *Mariner* Mars 1964 solar panel would produce a nominal output of 578 w for Sun-oriented operation in space at 135 mw/cm^2 solar irradiance and an isothermal cell temperature of 55°C. (Flight acceptance and launch degradation were neglected in obtaining the 578-w performance.) The *Mariner* Mars 1964 panel characteristics based on *Mariner 2* and *Ranger* type approval solar panel assemblies are compared in Fig. 6.

The improvement in performance achieved on the *Ranger* Block III solar panels, which is expected for the *Mariner* Mars 1964 solar panels, is a direct result of the procurement and independent screening of the solar cells to assure uniformity of output and the development of improved assembly processes, which are controlled by process specifications and in-process quality assurance inspection.

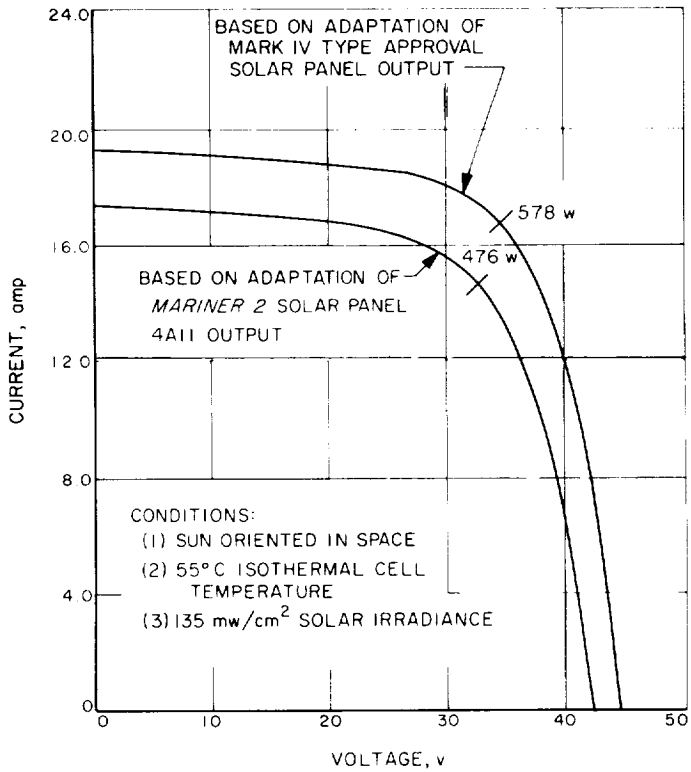

Fig. 6. *Mariner* Mars 1964 solar panel current-voltage characteristics

IV. *Voyager* Project

The primary objective of the *Voyager* Project is the scientific exploration of Mars and Venus by means of spacecraft designed for use with *Saturn* boost vehicles. Secondary objectives are the scientific exploration of interplanetary space in the Mars-Venus region, and the determination of the feasibility of the development of technology for, and the collection of scientific data necessary to successful manned flights to these planets.

The *Voyager* Project is currently in the planning phase. An Advanced Planetary Spacecraft Study Committee has been organized to determine possible mission objectives and design concepts of *Voyager* and later spacecraft for use on the *Saturn* class of boost vehicle. Conventional spacecraft designs as well as designs incorporating advanced propulsion techniques are being analyzed. Results to date indicate that the optimum mission for the *Voyager* class of spacecraft is probably a combination orbiter/lander. It is, therefore, this concept on which mission studies are being concentrated.

Power systems. Design studies on power systems capable of satisfying the requirements of the *Voyager* spacecraft are in progress. Nuclear and solar systems with several types of converters are being considered for the orbiters. Nuclear radioisotopes with thermoelectric converters and chemical primary batteries appear attractive for the landing capsules.

Propulsion systems. A study has been made of the propulsion requirements for the landing capsule of an orbiter/lander mission. Propulsion systems on board the capsule may be required to provide velocity increments for three purposes: (1) deflection of the capsule to an impact trajectory, (2) acceleration of the capsule for arrival-time adjustment, and (3) cushioning of the capsule touchdown.

Three propulsion systems have been presented for consideration for the *Voyager* mission. These are: (1) a sterile cast and assembled solid motor, (2) a heat sterilizable solid motor, and (3) a heat sterilizable bipropellant liquid.

The heat sterilizable solid motor has been recommended for the *Voyager* capsule, assuming the proposed

THE DEEP SPACE INSTRUMENTATION FACILITY

V. Introduction

The DSIF is a precision tracking and data acquisition network which is designed to track, command, and receive data from deep space probes. It utilizes large antennas, low-noise, phase-lock receiving systems, and high-power transmitters at stations positioned approximately 120 deg around the Earth. Its policy is to continuously conduct research and development of new components and systems and to engineer them into the DSIF so as to continually maintain a state-of-the-art capability.

The DSIF is comprised of three permanent deep space stations, one mobile station, and one launch station. The three permanent stations are located to provide continuous coverage of a deep space vehicle. Their locations are Goldstone (Pioneer and Echo), California; Woomera, Australia; and Johannesburg, South Africa. The Mobile Tracking Station (MTS) is presently located near the permanent station in South Africa and is used mainly for early acquisition, and tracking and communications with spacecraft from injection into orbit to an altitude of about 10,000 mi. The Launch Station is used to provide real-time telemetry during the spacecraft prelaunch tests and to record spacecraft transmitted telemetry data from launch to the end of the visibility period.

The testing and development engineering of new equipment for the DSIF are performed at the Goldstone Space Communications Stations. In most cases new equipment is installed and tested at Goldstone before it is integrated into the system. An 85- and a 30-ft Az–El antenna are installed at the Goldstone Venus site for primary use in research and development.

Section VI of this Report, regarding the DSIF Program, is abstracted from *SPS 37-22*, Vol. III.

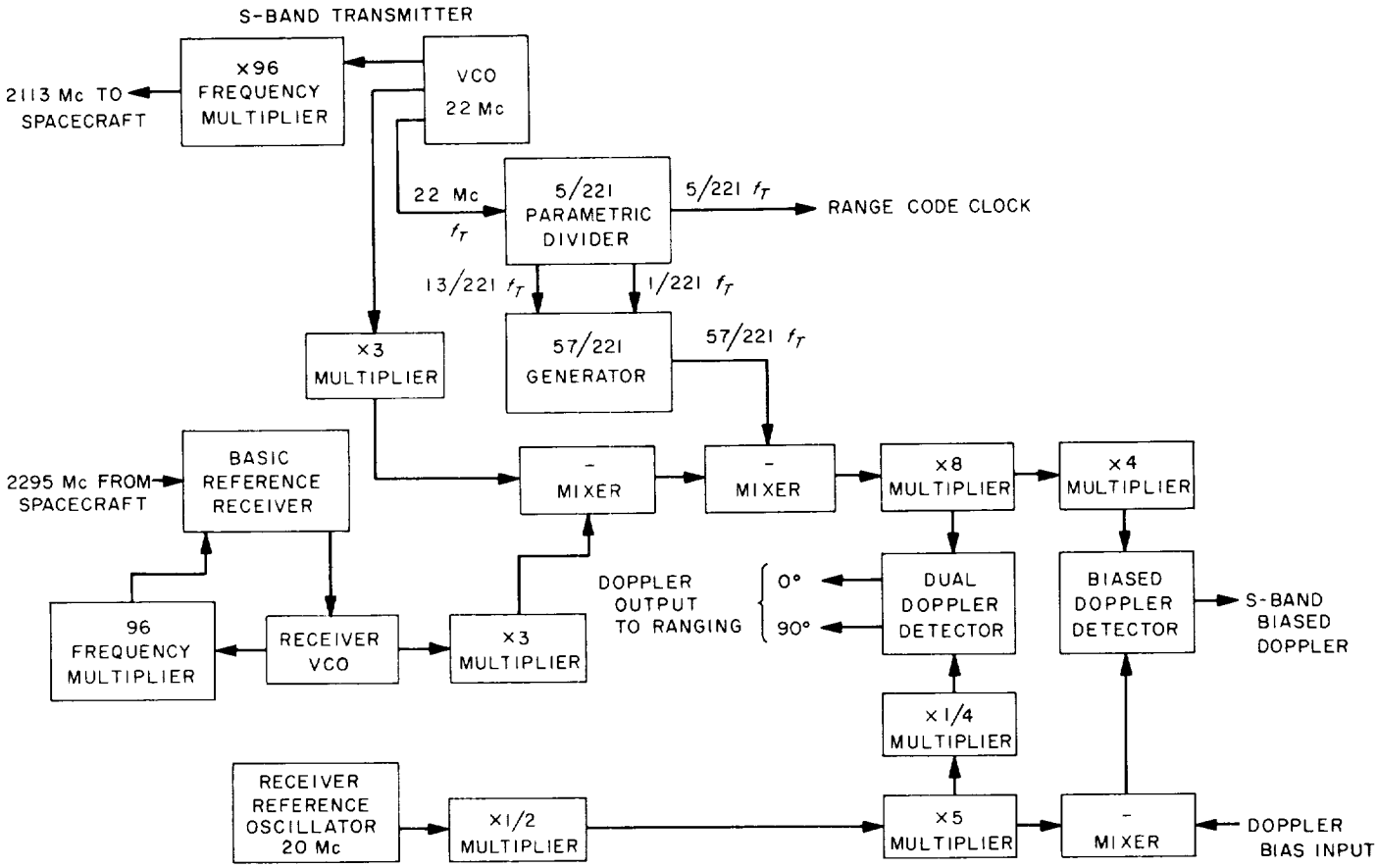

Fig. 1. Coherent range clock and RF doppler design system

Basically, the 5/221 unit consists of two parametric frequency dividing circuits in tandem. The first provides an output which is 1/17 of the 22-Mc input frequency. The second, a divide-by-13, provides an output which is 1/221 of the 22-Mc input frequency. This signal is then multiplied by five to provide a coherent 5/221 output. The output of each divider is also utilized in the coherent doppler chain. The block diagram shown in Fig. 1 indicates the relative position of the 5/221 frequency divider within the RF system.

B. Research and Development

Experimental low-noise system. The development of a traveling wave maser for the DSIF is essentially complete with all specifications being met except that of noise temperature. However, the approach to be taken in a future program to reduce the noise temperature is understood. Pertinent performance specifications are noise temperature 16 ± 2°K, gain 30 ± 1 db, and 1-db bandwidth, 11 Mc. The closed cycle refrigerator was found to be satisfactory for field operation.

Ground antennas. The servo system on the 30-ft antenna at the Goldstone Venus site is still under test. As installed, the minimum tracking rate is 0.10 deg/sec. This is too high for pattern measurement work and a temporary modification, including servo valves, has been installed which reduces this rate to less than 0.004 deg/sec.

The Mount Tiefort S-band antenna range was successfully used to make antenna pattern measurements of the 85-ft Az–El antenna at the Goldstone Venus site. A standard horn antenna whose gain had been carefully measured by two independent methods was used on Mount Tiefort. The gain of the 85-ft antenna was found to be 54.01 ± 0.15 db at 2388 Mc. The measurements indicate that the Mount Tiefort range is essentially free

In order to partially automate the technique of using astronomical radio sources for boresight and gain calibrations of 85-ft antennas, a sequencer has been developed, so that pertinent data can be recorded in a format which is compatible with the Model 1620 digital computer. The station data handling equipment is used to generate the punched paper tape and printer output with the normal locations of the doppler data being used for the digital reading of the output of the Dicke radiometer. The computer program for reducing the data is nearly complete.

In order to use astronomical radio sources for antenna calibrations, it is necessary to know the noise temperature and polarization characteristics of these sources. Careful measurements of source intensities and polarizations have been made on 14 sources including the Moon and the Sun. The first results of this data show that the Crab Nebula should be very useful since it has relatively high intensity, is small in diameter, and is only slightly polarized. The Moon, Sagittarius, and NGC 5128 are not so useful because of their large diameters.

The new design of a water rotary joint appears to be satisfactory. Dynamic and life testing at JPL will be conducted as soon as the vendor completes one unit.

Ranging system development. The stored program controller in the Mod II ranging equipment now has all the capabilities necessary for completely automatic control of ranging operations. It has many of the characteristics of a small general purpose computer. Capabilities which have been added recently include the arithmetic operations of shift, multiply and divide, the control function of program interrupt, and a printer and paper tape punch as peripheral equipment.

A total of 18 test program routines has been written which will determine the operational capability of the stored program controller. Additional programs will be written which will make it possible to test all parts of the machine.

Acquisition of a telemetry modulated RF carrier by a phase-lock receiver is generally susceptible to spurious sideband locking effects. A subsystem capable of discriminating against virtually any type of modulation which is suitable for modulation of a tracked carrier has been developed and subjected to preliminary tests. Primary limitations of the discriminator are:

(1) Signal strength must be somewhat above predetection threshold.

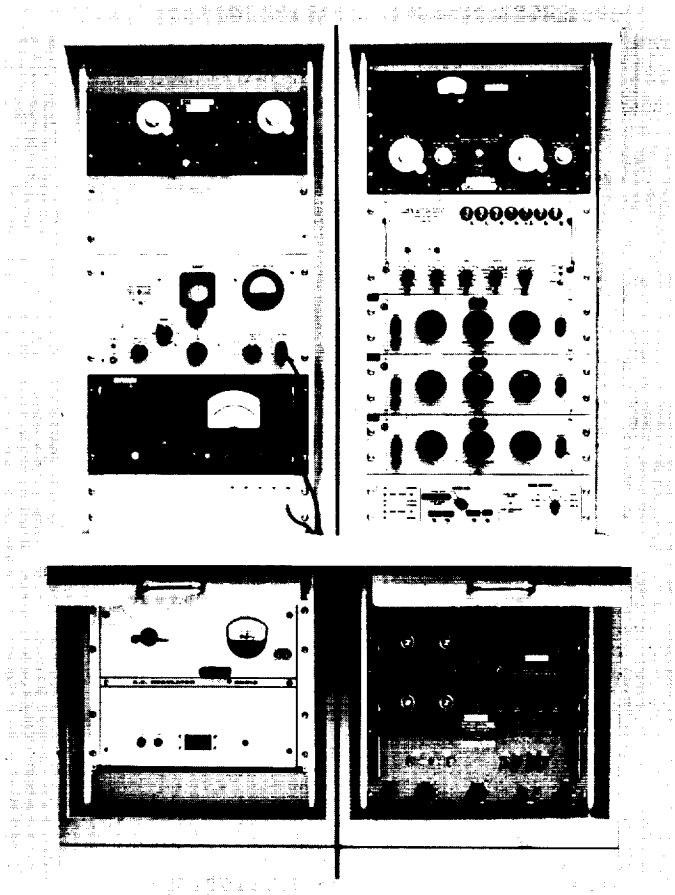

Fig. 3. Precision signal and noise mixing system

(2) Fundamental frequency of any subcarrier must exceed the loop bandwidth but not exceed the predetection bandwidth.

Data signal discrimination. In order to test the performance of a detection system where a data signal is mixed with white gaussian noise, a mixing system has been designed, constructed, and tested. It is linear over a wide range of signal and noise levels and has a frequency response of ± 0.1 db from 10 cps to 100 kc. Fig. 3 is a photograph of the completed system.

C. Facilities

Advanced Antenna System. A contract for the final design, fabrication, and erection of a 210-ft parabolic antenna at Goldstone has been executed with the Rohr Corporation of Chula Vista, California.

OPERATIONAL AND TEST FACILITIES

VII. The Space Flight Operations Facility

The Space Flight Operations Facility (SFOF) is being developed at JPL to provide spaceflight operational, technical and support functions required for the conduct of future unmanned lunar and planetary–interplanetary spacecraft missions. During operations, the facility and participating remote tracking and communications stations will function as a single information handling, analysis, interpretation, evaluation and command network, and will include extensive data processing and decision making capabilities. A summary presentation of the over-all SFOF physical configuration, functional capabilities and associated supporting activities was presented in *SPS 37-20*, Vol. VI, pp. 43–67.

A. Space Science Analysis Area

The Space Science Analysis Area (SSAA ; Fig. 1) is one of the technical areas within the Space Flight Operations Facility (SFOF). The function of the SSAA is to monitor, evaluate, and report scientific data received from space missions. In addition, the SSAA operates commands affecting scientific experiments.

As previously stated (*SPS 37-20* and *-21* Vol. VI) for other SFOF areas, the SSAA development will be an evolutionary process; that is, as experience is gained through use of the initial complement of equipments and/or new requirements arise, these equipments will continually be changed to provide maximum utilization and reliability.

1. Data Processing and Display System

The SSAA receives raw data via teletype printers from the communications terminus and processed data from the IBM 7094/7040 computer complex via plotters and printers. Access to the digital data system is achieved through a remote input/output console within the SSAA. The console provides the capability to monitor and/or alter programs in the computing complex.

Two categories of displays are contained in the SSAA. One consists of manual and semi-automatic displays for internal use within the SSAA. The other is for internal use or to be remoted to other areas.

a. Displays for internal use of the SSAA.

Engineering sensor display (Fig. 2). This display provides for viewing sensor status, most current values, apparent trends, and predetermined data boundaries.

The display is divided in half with 10 rows of information per half. In the upper 10 rows, the sensor title, units and remarks columns will employ replaceable name plates or chalk; the status, trend, and alarm columns will employ remotely selectable lights; and the value and boundary columns will employ remotely selectable six-digit numeric indicators. In the lower 10 rows, the format will be identical to the upper 10 rows except that the value and boundary columns will employ replaceable numeric characters or chalk.

Science sensor display. This display will be a metal-backed blackboard employing magnetic backed characters or chalk throughout. The display shown in Fig. 3

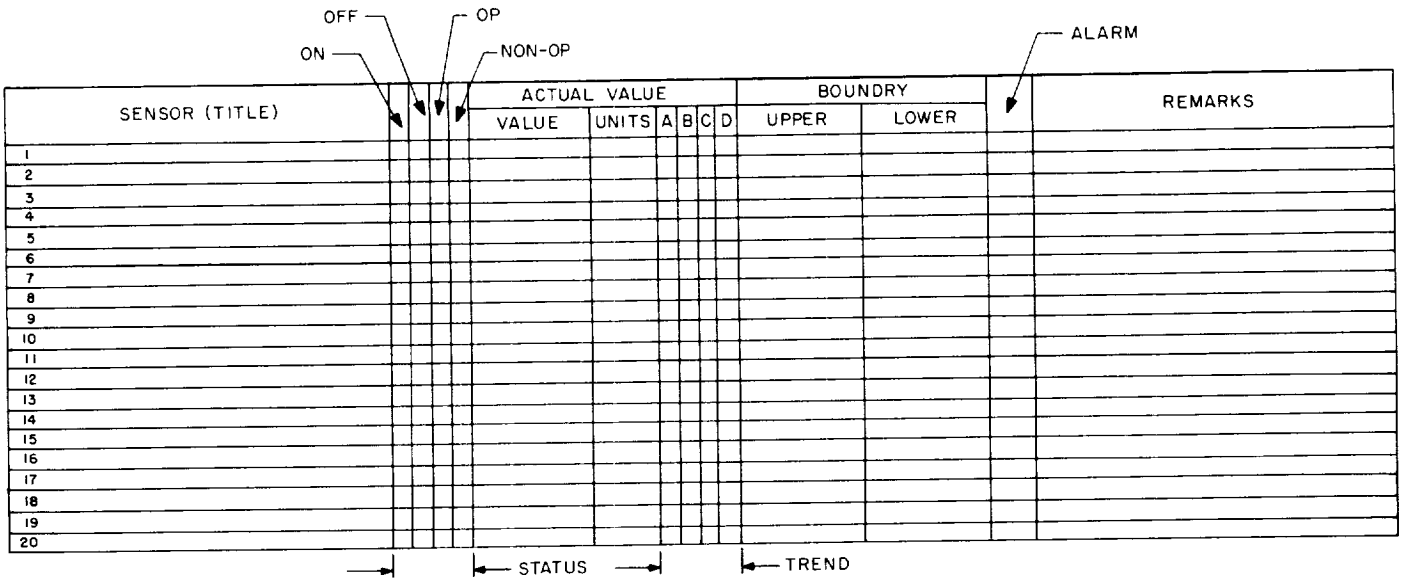

Fig. 2. Engineering sensor display

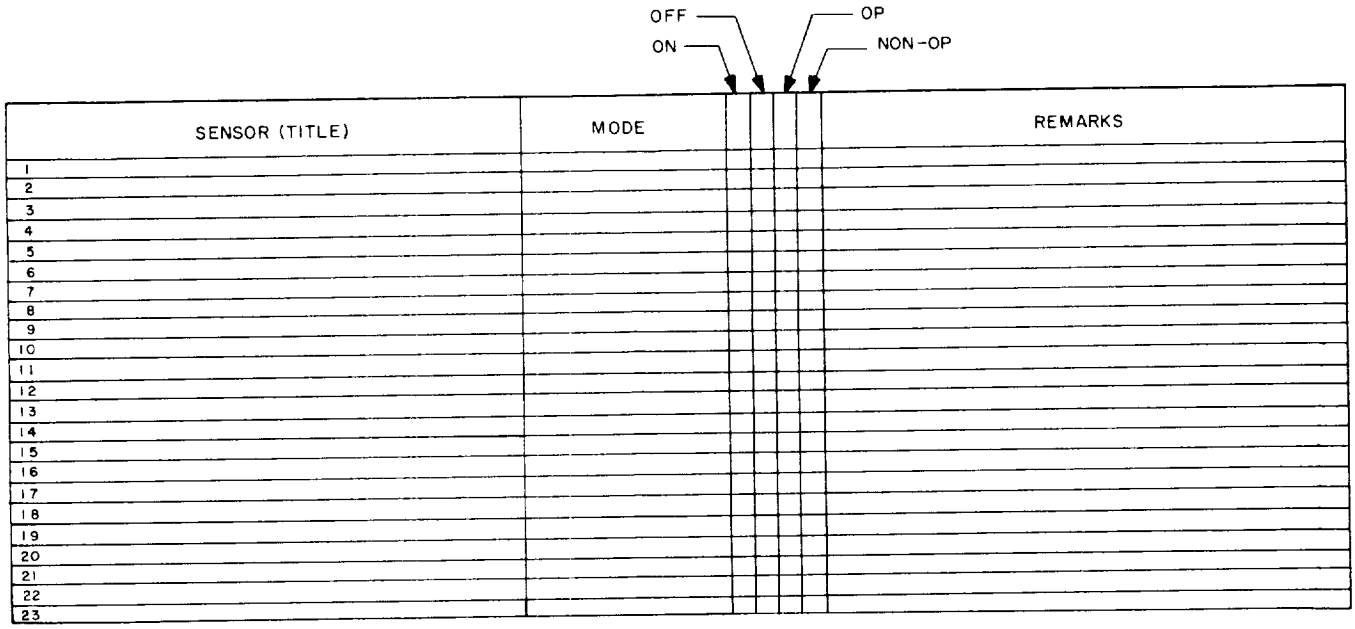

Fig. 3. Science sensor display

Table 1. Remote displays for Space Science Analysis Area

Description	Originating area
Spacecraft command, Mission 1	Mission control
Spacecraft command, Mission 2	Mission control
Mission direction, Mission 1	Mission control
Mission direction, Mission 2	Mission control
Semidetailed SPAA information	SPAA[a]
Semidetailed FPAA information	FPAA[b]
DSIF system status	Mission control
SFOF operational status	Mission control
GMT and mission dependent time (two monitors)	

[a]SPAA: Spacecraft Performance Analysis Area.
[b]FPAA: Flight Path Analysis Area.

A Moon mosaic display and slide projector analysis display (Fig. 1) are contemplated after Stage II of the SFOF development is complete.

B. Communications System

The Communications System of the SFOF, as reported in *SPS 37-20*, Vol. VI, is composed of a number of subsystems associated with the different media employed in the SFOF. Each of these subsystems will be reported individually in separate issues of the *SPS* in order to allow full technical presentations.

1. Operational Voice Communications Subsystem (OVCS)

a. General description. The OVCS provides the voice communications within the SFOF, and between the SFOF and operational and nonoperational agencies outside the SFOF. The OVCS is composed of three integrated subsystems:

(1) An intercom subsystem that will be the primary means of voice communications within the SFOF.

(2) A telephone subsystem that will provide intra-SFOF voice communications and the primary means of communicating between the SFOF and nonoperational and some operational agencies outside the SFOF.

(3) A conference subsystem that will provide the voice communications within the SFOF and with other operational agencies outside the SFOF.

Operation of the OVCS is achieved by the use of standardized subsystem functional modules. These subsystem modules are combined in various configurations for both console and desk mounting to meet the communication needs of each operating position. Thus, from a minimum number of equipments, the optimal capability is achieved at each operating position.

b. Intercom subsystem. The intercom subsystem is directly selectable, provides microphone/loudspeaker operation, and can be operated without the use of any hand or foot controls. It provides a signal lamp to indicate an incoming call, an alternate headset mode of operation, conferencing capabilities, and an optional priority break-in feature. The intercom subsystem also provides (on an authorized basis) access to the general-page and local-page channels of the SFOF public address subsystem. The intercom subsystem uses direct station-to-station wiring that is independent of both the telephone subsystem and the conference subsystem; this greatly increases the traffic handling capabilities of the OVCS.

c. Telephone subsystem. The telephone subsystem consists of a special telephone instrument and two groups of lines, SFOF and auxiliary. The SFOF lines are restricted to the OVCS only and provide a telephone system for the exclusive use of operational traffic. The auxiliary lines connect to the JPL administrative telephone system and provide a link to the rest of the Laboratory and local and long distance service.

The telephone subsystem also provides for the direct establishment of three, four, or five party conference by any subsystem user. A long distance call may be included in a conference if it is established with the auxiliary lines.

d. Conference subsystem. The conference subsystem is a four-wire nonsignalling telephone system that has the initial capability of handling simultaneously 19 conferences, each of which can be associated with one or more external four-wire voice channels from multiplexing equipment, leased long-distance lines, or other sources. Each conference network has the capability of handling 200 or more user stations within the SFOF.

Two types of end instruments are available to the user for connection to these conference networks, speakers and headsets. Individual and separate selector modules are provided for each of the instruments.

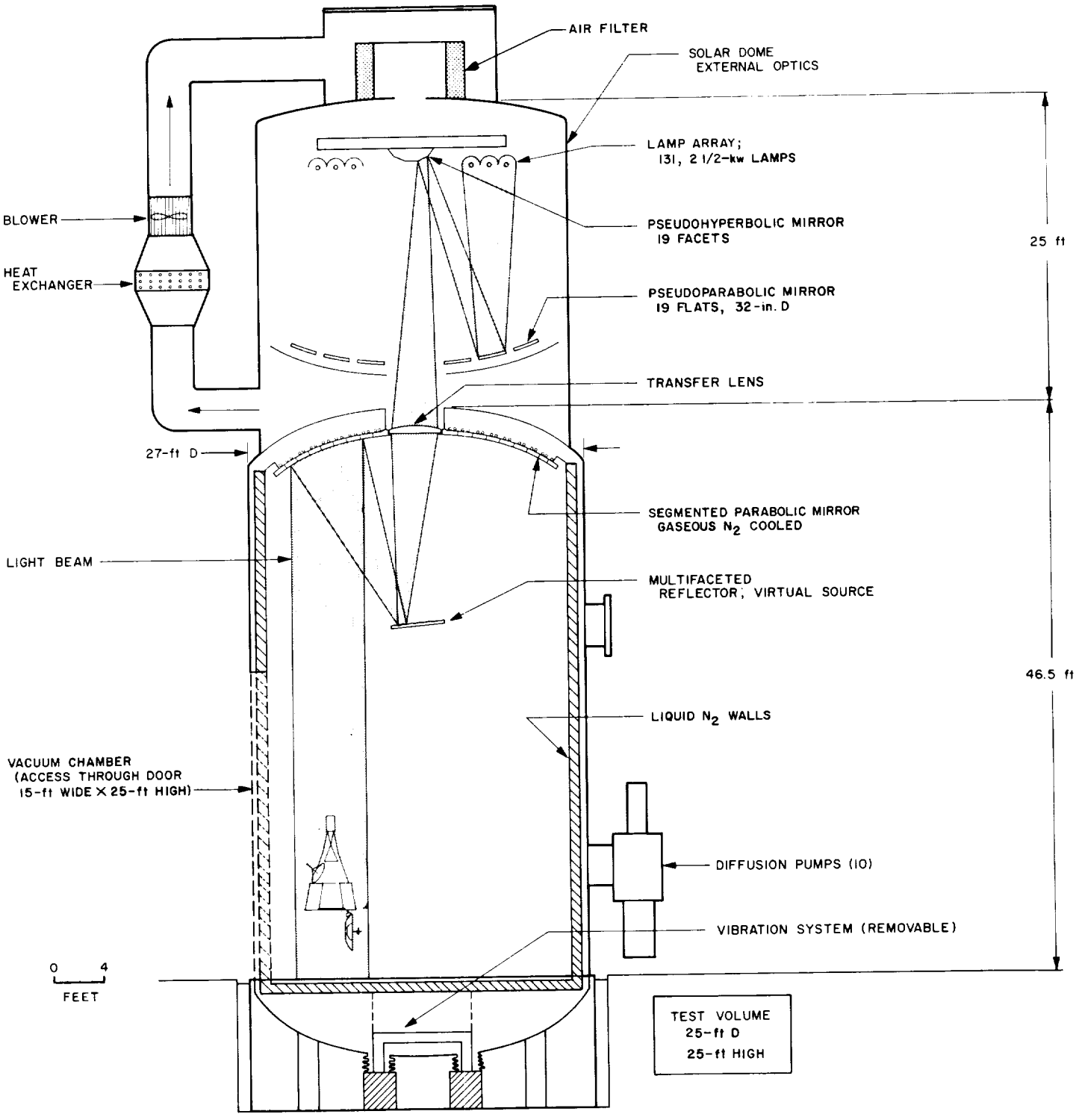

Fig. 1. JPL 25-ft Space Simulator

Positioner. For positioning, a machine is used which is capable of rotating the spacecraft in pitch and roll in order to provide favorable attitudes for assembly and systems test. When the spacecraft is mounted on the positioner, most of the assembly work can take place at a plane which is about waist-high above the floor.

SPACE SCIENCES

IX. Space Instruments Development

A. Gas Chromatograph Detector Quiescent Current Drift Compensation

1. Introduction

Most sensitive ionization detectors used with gas chromatographs possess a quiescent current large compared to the currents produced by eluted samples. Since this quiescent current is dependent on temperature, pressure, and ionization source intensity, the current cannot be assumed to remain fixed over long periods of time. Therefore, the measurement of small concentrations by a gas chromatograph which must operate after several months of space flight necessitates an automatic base-line compensating scheme.

For example, the difference of the currents from two identical detectors, one of which receives only carrier gas, would only be contributed by the eluted sample. However, because the detector quiescent currents would have to remain matched to better than 0.1% for nearly a year, small variations in source intensity, carrier gas flow rate, or detector dimensions could not be tolerated.

Alternatively, the detector quiescent current could be cancelled electronically by adding an equal but opposite current to the electrometer input, assuming that the quiescent current remains constant while the sample is being analyzed. One such technique (*SPS 37-20*, Vol. IV, p. 169), consisting of a comparator amplifier with a low-pass filter, proved to have the disadvantage that the detector current peaks charged the capacitor in the low-pass filter resulting in undershoots following the peaks. In order to prevent these undershoots, the compensating system could be disconnected while the chromatogram is being run, and the base line compensating current supplied from a storage system which set the electrometer output to zero just before the sample was run. One such storage system using capacitors, resistors, and reed switches is discussed below.

Thus, typically for:

$$I_{max} = 10^{-9}\,\text{amp}$$

$$I_{min} = 10^{-12}\,\text{amp}$$

$$C = 4\,\mu\text{f}$$

$$V_s = 20\,\text{v}$$

then:

$$T = 80\,\text{sec} \tag{5}$$

3. Double Resistance-Capacitor Storage

In order to increase T, the slightly more complicated scheme of Fig. 2 is proposed. Before the chromatogram is run, the reed switches are closed, charging C_1 and C_2 to V_{10} and V_{20}, respectively, and zeroing the electrometer. The compensating current i_2 then decays according to the following formula:

$$i_2 = \frac{V_{20}(\tau_1 + \alpha\tau_2)}{R_1}\left[\frac{1 + \frac{p\alpha\tau_1\tau_2}{\tau_1 + \alpha\tau_2}}{1 + p\left(\tau_1 + \frac{\tau_1 + \tau_2}{\beta}\right) + \frac{p^2\tau_1\tau_2}{\beta}}\right] \tag{6}$$

where:

$$\alpha = \frac{V_{20}}{V_{10}} = \frac{R_4}{R_3 + R_4}$$

$$\beta = \frac{R_1}{R_2}$$

p = Laplace transform variable

$$\tau_1 = R_1 C_1$$

$$\tau_2 = R_1 C_2$$

This formula can also be written

$$i_2 = \frac{V_{20}}{R_1}(\tau_1 + \alpha\tau_2)\left(\frac{1 + p\tau_n}{1 + pb + p^2c}\right) \tag{7}$$

where:

$$\tau_n = \frac{\alpha\tau_1\tau_2}{\tau_1 + \alpha\tau_2}$$

$$b = \tau_1 + \frac{\tau_1 + \tau_2}{\beta}$$

$$c = \frac{\tau_1\tau_2}{\beta}$$

The inverse transform gives the function:

$$i_2(t) = \frac{V_{20}(\tau_1 + \alpha\tau_2)}{R_1(\tau_+ - \tau_-)}\left(\frac{\tau_+ - \tau_n}{\tau_+}e^{-t/\tau_+} + \frac{\tau_n - \tau_-}{\tau_-}e^{-t/\tau_-}\right) \tag{8}$$

where:

$$\tau_+ = \frac{b + (b^2 - 4c)^{1/2}}{2}$$

$$\tau_- = \frac{b - (b^2 - 4c)^{1/2}}{2}$$

Expanding Eq. (8) to second order in t:

$$i_2(t) \cong \frac{\alpha V_{10}}{R_2}\left[1 + t/\tau_L - \tfrac{1}{2}(t/\tau_Q)^2\right] \tag{9}$$

where:

$$\tau_L = \frac{c\tau_n}{c - b\tau_n}$$

$$\tau_Q^2 = \frac{\tau_n c^2}{bc + \tau_n(c - b^2)}$$

The first approach to optimizing this technique is to remove the linear term in the decay by selecting τ_n (by choosing α) so that $\tau_L \to \infty$. For this case:

$$\tau_n = c/b \tag{10}$$

Substituting the values of c and b, the condition on α becomes

$$\alpha = \frac{1}{1 + \beta} \tag{11}$$

and τ_Q^2 may be written as:

$$\tau_Q^2 = C_1 C_2 R_1 R_2 \tag{12}$$

If the total capacity C_0 available and dynamic range V_s of the comparator amplifier are considered fixed then:

$$C_1 + C_2 = C_0$$

$$I_{max} = \frac{\alpha V_s}{R_2} = \frac{V_s}{R_1 + R_2} \tag{13}$$

and the maximum value of τ_Q occurs for:

$$C_1 = C_2 = \tfrac{1}{2}C_0$$

$$R_1 = R_2 = \frac{V_s}{2I_{max}} \tag{14}$$

4. Conclusion

From Eq. (30) it is apparent that the rather simple circuit of the double resistance-capacitor storage is capable of preventing drifts in excess of 10^{-12} amp for periods of over 30 min. If an electrometer feedback resistor R_1 of 10^{10} ohms were used, then a 10^{-12}-amp drift corresponds to 10 mv at the electrometer output. This drift is equal to the stability of the electrometer and of the present comparator amplifier. Thus, the system would be well optimized for a threshold signal level of 10^{-12} amp.

The storage time of 30 min exceeds the length of any anticipated chromatogram and probably exceeds the length of time for which the detector should be assumed stable.

The actual mechanization of such a capacitor storage is proceeding, and a report is expected in the future on a chromatograph making use of this principle.

B. Minimizing Picture Data With Planetary Pictures

1. The Planetary Mission

In a planetary mission where the space science experiments to be conducted include optical surface-feature exploration, the resultant data will be mostly picture information. A need thus arises for reliable and accurate techniques that will minimize the picture data. Generally the aim of these techniques is to eliminate redundancy. However, if in introducing any of these methods, inaccuracies or partial loss of resolution occur, then the process would be generally unacceptable for exploratory planetary uses. The resolution in question would be that specified by the cognizant experimenter in relation to the mission objectives.

2. Resolution Criteria

The surface features of a planet may be electronically photographed from a passing spacecraft with a slow-scan vidicon camera. The information that is contained in the vidicon charge-image area is converted into a time-dependent function by sampling. The information content, H bits/picture, is determined from the resolution specified by the experimenter, the area to be observed, and the system capacity, $C = B \log_2 n$ bits/sec. In terms of the corresponding resolution element that becomes established for the system, the information content of the sampled signal will be less than the information content of the charge image due to the sampling process. This does not present a problem as it is the sampled image and not the charge image that forms the basis of the experimenter's criterion. However, it must be recognized that the experimenter's criterion is formed on the assumption that there are no significant sampled-data errors, and that no degradation arises in the reassembly of the picture from the information supplied by the data link. All image operators are assumed to be linear and the data is assumed to be transmitted and reassembled in an orderly manner.

If processes are introduced into the system so that the data cannot be reassembled in an orderly and linear manner, i.e., random or non-linear processes are introduced, then the problems of picture reconstruction are greatly increased. A computational machine may then have to be inserted into the system to reduce all data into a form that is linear and orderly for the purposes of picture reassembly. The need for such a machine may not only reduce the accuracy of the planetary information, but may be economically and logistically undesirable in relation to a mission that is exploratory in nature.

3. The Matrix Assembly

A true electrical signal corresponding to the optical image can only be obtained from the vidicon when there is motion between the scanning beam and the charge image. Thus, only when the beam is driven across the image at constant velocity is a true electrical signal in the time domain produced. For a stationary beam the output is zero. If all other operators on the charge image are linear and orderly, the sampling and digitizing processes will produce a linear, solid-digital-matrix assembly. The matrix assembly is built from an arrangement of picture element modules of dimensions x, y, z where $x = \Delta t$, $y =$ the scanning line pitch, and $z =$ the element intensity in digital notation. Here $\Delta t = 1/2f_c$; and f_c is the amplifier cut-off frequency. A reversal of the process transforms the time-domain information back into x, y, z coordinates for visual observation. The whole of the picture area is constituted by an orderly array of data where a black area comprises an orderly array of zeros

(2) terminator views of high contrast. The information content is expected to be random. It is customary to employ lunar transparencies for flight camera performance evaluation. However, logically arranged test patterns are also employed. The information derived from the test charts is thus no longer random but highly organized and periodic. If periodic functions are intermeshed and visually presented, moiré patterns appear. For example, when the periodic line sampling process is interleaved with a horizontal bar charge-image produced by the test pattern, a moiré pattern appears. This is demonstrated by the reproduced picture of the horizontal wedges in Fig. 5(a). A moiré pattern created in the vertical direction by picture element sampling is shown in Fig. 5(b). When the scanning lines sample a scene having random characteristics as with a planetary view, there is no moiré pattern. However, if a second sampling process is introduced, moiré patterns may reappear even if the scene is random. For planetary surface analysis the introduction of moiré patterns due to sampling or reassembling processes must be considered undesirable.

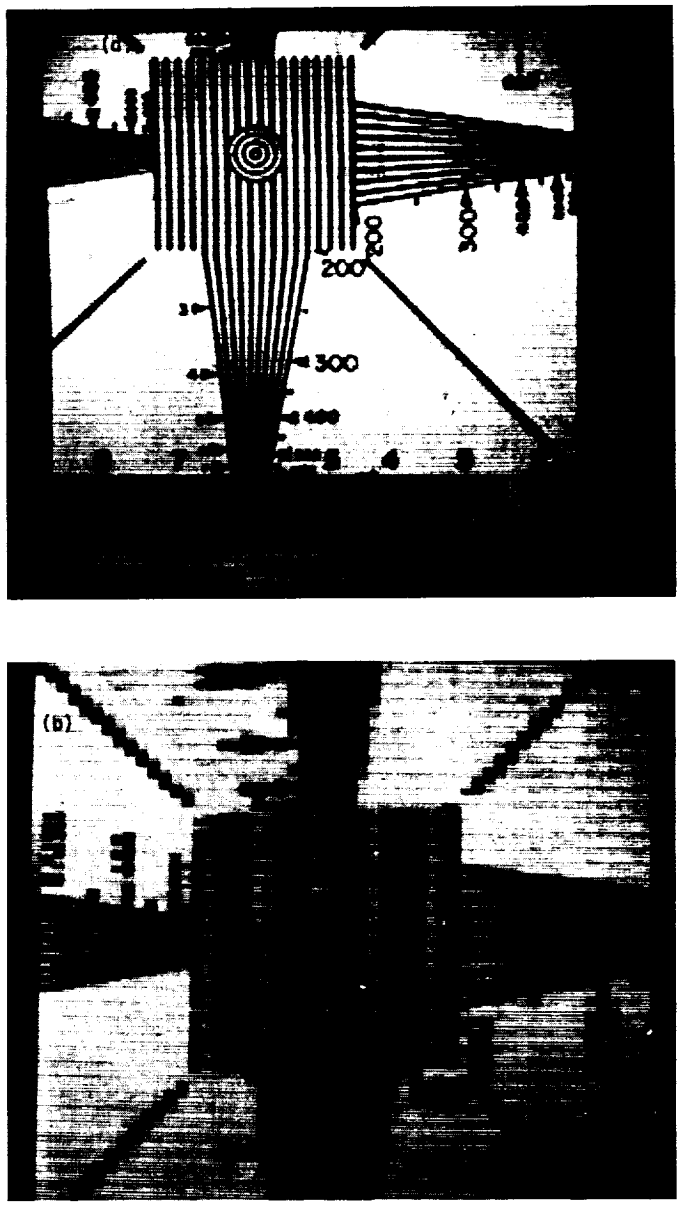

Fig. 5. Moiré patterns

7. Rep-2 Sampling

When picture element sampling is introduced to produce a digital matrix assembly, the problem arises of how best to arrange the sampling. The sampling process should include considerations of the final picture reassembly. For example, in broadcast TV the line sampling is interleaved in order to minimize flicker in the reassembled display. The simplest method of element sampling is to sample each element sequentially. However, if there is low picture information content an every-other-element sample or less may be adequate. In this case, holes will appear in the matrix. One process for eliminating the holes is to duplicate the information from adjacent elements. This may be accomplished, for example, by a sample-and-hold technique duplicating the data from the previous sample. This is the method used for presenting complete picture data in the sampled pictures shown.

Straightforward every-other-element sequential sampling produces a sampling pattern having $n/2$ sampled point arrays where n is the number of scanning lines. However, a more advantageous distribution of points is obtained if the sampled elements are shifted one element at every line. This may be explained by considering each element to be a mathematical point and investigating elemental areas covered by these points. For continuous sequential sampling four interconnected points on adjacent lines are seen to enclose a 1×1 square. When sampling every other point the four points enclose a 1×2 rectangle. If the elements are shifted one element each line then the four points now enclose a $1 \times (2)^{1/2}$ polygon as shown in Fig. 6. The last can be recognized as a rep-2 polygon in contrast to the two previous examples, which are rep-4 polygons (*SPS 37-18*, Vol. IV, pp. 149–154). The $1 \times (2)^{1/2}$ polygon is the only known rep-2 four-sided polygon. The rep-2 polygon distribution produces an array of sampled points having $(n - 1)$ lines spaced diagonally across the picture as opposed to $n/2$ arrays spaced vertically with sequential sampling.

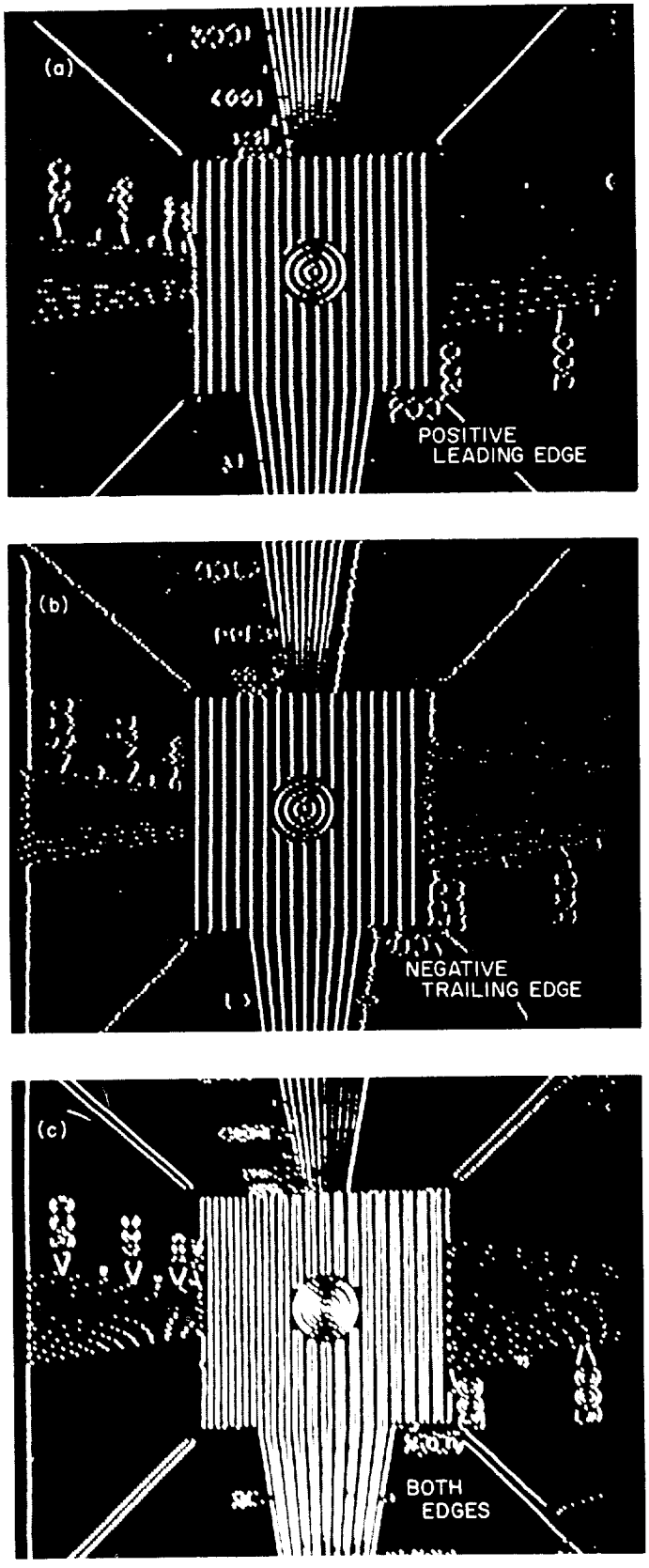

Fig. 9. Edge sampling with test pattern

Fig. 10. Loss of edge signals due to indeterminate Δz

areas in a picture are located in the edge regions where an edge may be defined by the magnitude and polarity of dz/dt. If noise is significant, then, since the characteristics of the noise are similar to those of the signal, dz/dt will also define noise pulses. The relative amplitudes of the two signals will determine to what exent an edge is differentiated from a noise pulse. Prime picture information regions are illustrated in Fig. 9, which is an $x - y$ plot of dz/dt for a test pattern. Figs. 9(a) and 9(b) show the locations of the positive and the negative edges where positive and negative are defined by the polarity of dz/dt. Fig. 9(c) shows the two sets of edges combined to form a complete assembly of edge information points. The indeterminate resultant when Δz is digitized is demonstrated by the loss of edge information following digitization of the same test pattern shown in Fig. 10. Fig. 10 may be compared with Fig. 9(c); attention is directed toward the diagonal lines where the information loss by digitization is more apparent. Edge sampled data for a random signal is presented in Fig. 11 for three levels of signal/noise discrimination. The random signal is a picture of a Moon crater. There are 1600 sampled data elements in Fig. 11(a), 3100 in Fig. 11(b) and 15,000 in Fig. 11(c). A fully sampled picture would contain about 35,000 elements. Using the sample-and-hold technique, the picture is reassembled from the edge data of Fig. 11(b) and is presented in Fig. 12. While the essential features are preserved with a reduction in data of over 10 to 1, much of the fine detail is lost. Considerable improvement could be made, however, using a picture reassembly technique that employed interpolation rather than the simple sample-and-hold technique used for these experiments.

bath, a resistive substrate upon which metal is deposited, and a metal source electrode. Two leads are attached to the substrate. The resistance between these leads can be reversibly controlled by passing a DC plating current into the third lead. As long as a current is passing through the third lead, the resistance will scan through its range. Once the current is reduced to zero, the resistance will remain substantially constant. Hence, the memistor operates as an integrator since the resistance between two of the leads is governed by the total charge flow rather than by the instantaneous current in the third lead. A schematic of the device is shown in Fig. 13.

According to Faraday's law, the amount of metal plated is precisely proportional to the integral of the plating current. The conductance C then of the memistor is the sum of the unplated conductance and the conductance of the deposited metal film. Since the latter is proportional to the amount of metal plated, the conductance may be expressed as

$$C = C_0 + K \int i dt$$

$$C_0 = 0.02 \text{ mho}$$

$$K \approx 25 \text{ mhos/coulomb}$$

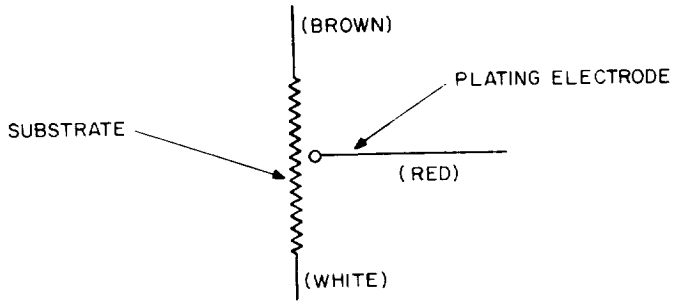

Fig. 13. Memistor schematic

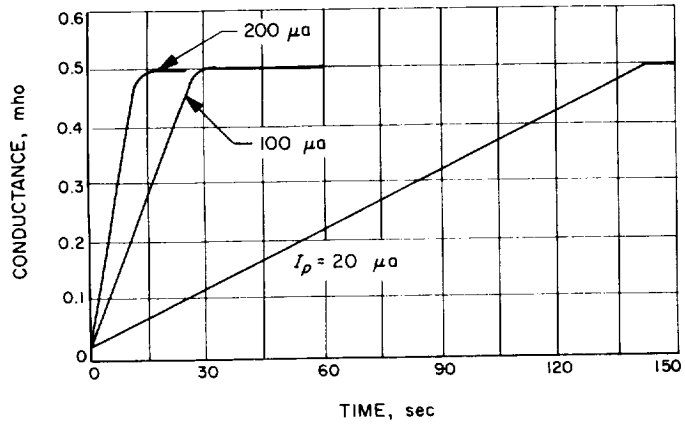

Fig. 14. Memistor plating characteristics

Saturation takes place when the substrate is heavily plated. Fig. 14 shows the constant current plating characteristic for the device.

In the application presented, the memistor would be implemented as shown in Fig. 15. The voltage E should be a symmetrical wave form with respect to ground, preferably a sine wave, since any DC component applied to the memistor substrate will cause some plating. The excitation frequency can be anything from 60 cps to several megacycles. The conductance of the memistor is non-destructively sensed by the voltage e_s.

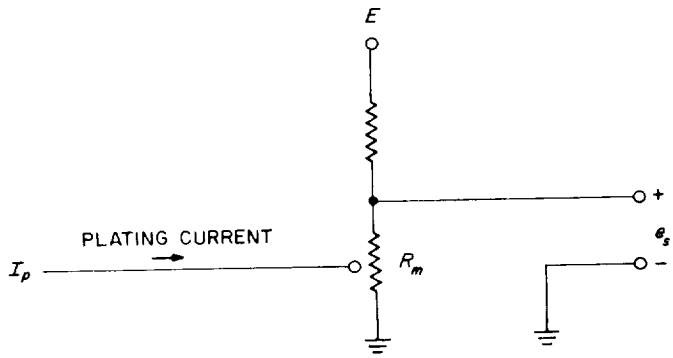

Fig. 15. Memistor implementation

2. System Operation

In the operation of the position servo, an AC voltage is generated, amplified, and converted into a DC voltage proportional to the initial background light level. From this the proper subtraction current is derived (Fig. 16). If the subtraction current I_s is first assumed to be zero, then the scattered light will cause a photometer current I_p to flow from the log amplifier. This current will cause the amplifier to have some output voltage between 0 and 5 v. This is the system output voltage. This output is also fed to the plating amplifier having a bipolar output with an adjustable offset. Any time the system output voltage is not equal to the offset voltage, there will be a corresponding correction voltage from the plating amplifier. This correction voltage from the plating amplifier causes a bi-directional current to flow as shown in Fig. 16, which causes the memistor R_m to change value. Its range is about 2 to 30 ohm. The memistor forms one arm of a resistance bridge while another fixed resistor equal to the minimum value of the memistor is used in another arm as shown. This will allow the pickoff voltage e to vary over a required three decade range. This allows the subtraction current a three decade range of variation

3. Bridge Oscillator

The oscillator is a conventional Wien bridge type. A field effect transistor is used as an input device for the amplifier section. This gives required isolation between the frequency selection bridge and amplifier section. Another field effect is used in an AGC loop to control the amount of degenerative feedback. Although the oscillator is still under development, frequency and amplitude stabilities of less than 1% over a temperature range of 0 to 60°C have been obtained.

4. Memistor Amplifier

This amplifier is a two-stage differential amplifier with AC coupling to the input. The AC coupling is used to prevent memistor plating due to input transistor DC bias currents. This plating could cause changes in memistor resistance, hence errors in the subtraction current. Symmetrical feedback is employed to control the voltage gain. Gain stability tests were performed on the amplifier. The results showed the amplifier gain to vary less than 0.5% over a temperature range of from −10 to +60°C.

5. Detector

The detector is a transistorized full wave rectifier driven by the bridge oscillator.

6. Memistor Stability

For this application long term (one week minimum) stability is of primary interest. Two factors which appear to affect the drift characteristics are:

(1) The current through the device used to generate a readout voltage. This current should be kept as low as possible since even with a plating current equal to zero and using a symmetrical excitation waveform, some plating does take place at one end of the substrate.

(2) The direction from which the desired resistance is set. For lowest drift, the selected value of resistance should be set from the fully plated or low resistance end.

Figs. 17 and 18 show typical short and long term drift characteristics. Two units selected at random are compared with six units selected for maximum stability at constant temperature. The reason for the drift is not fully understood; however, there is a possibility it may be due to partial plating due to the excitation voltage.

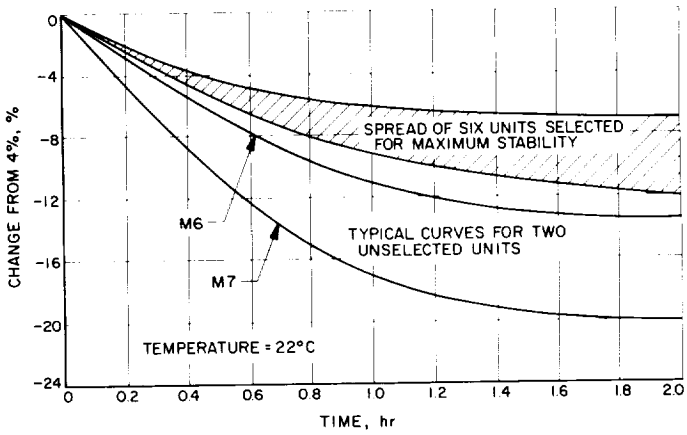

Fig. 17. Short term drift characteristic

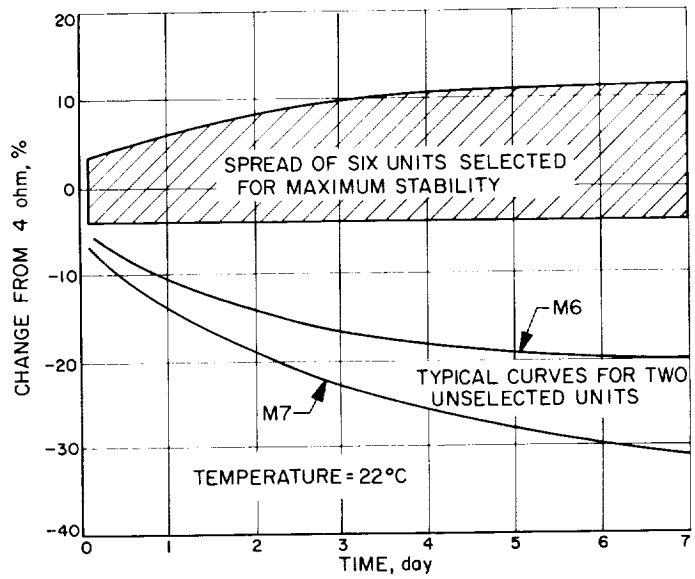

Fig. 18. Long term drift characteristic

D. TV Camera Shutter

The exposure time for the *Mariner* Mars 1964 TV camera is controlled by a rotating electromechanical shutter (*SPS 37-19*, Vol. VI, p. 81; *SPS 37-20*, Vol. VI, p. 112). The shutter, which is driven by a 25-w power solenoid, also operates as a color-filter wheel. Weight and power restraints imposed by *Mariner* Mars 1964 are reflected in the choice of a two-pulse drive as opposed to a single-pulse drive. In a two-pulse system the exposure is timed

two-pulse shutter circuitry in relation to possible logic errors introduced by switching transients. As a consequence, a number of circuit refinements have been added that will ensure positive electromechanical synchronization under any conditions expected in the evaluation or operation of the *Mariner* Mars 1964 payload. In addition, a simple backup redundant photo-cell device has been developed that will detect a spurious open shutter and rapidly reclose it. Arrangements are being made to permit this device to be inserted if unpredicted or uncontrollable conditions arise at some later phase in the program.

A complete shutter-wheel schematic diagram that includes the precautionary features discussed above is shown in Fig. 19. The original basic circuit philosophy was a minimum power and weight device that with a minimum number of components would energize a 25-w solenoid at logical intervals and synchronize the color-wheel with the internal logic. The maximum power taken at any time by the circuitry, including the 25-w solenoid drive, is 210 mw while the average power is of the order of 100 mw. The circuit is seen to comprise a 50-v power supply, two 660-μf discharge capacitors, two multivibrators, one for controlling exposure time, the other for controlling the solenoid-drive pulse-width, and three power transistor gates for controlling capacitor discharge times. The cam-operated microswitch S1 ensures synchronous color-wheel operation. One of the major design problems is to ensure that the 25-w solenoid switching functions do not interact with the logic timing functions.

The discharge capacitors must develop sufficient energy to sustain a high-current solenoid pulse during the exponential decay period. Capacitor weight is at a minimum when $W_c/W_s \rightarrow 1$ where W_c is the energy developed in the capacitor and W_s the energy required by the solenoid. For this circuit $W_c/W_s = 0.825/0.5 = 1.6$, a low ratio that requires adequate base drive at the power transistor gates to avoid switching inefficiencies. The gate drive originates in the timing multivibrators and to ensure isolation between the timing and driving functions, diodes CR21, 22, 23, and 24 have been added. To further optimize solenoid drive-power, the stabilizing zener-diodes across C13, 14 were removed as they reduce the capacitor potential, $W_c = Ce^2/2$. This is made possible as the capacitor voltage-breakdown rating had been increased from 50 to 75 v. To avoid switching transients from the microswitch, integrating networks R35 C9 and R41 C8 had been included. However, C8 resonated with the solenoid inductance at switch closure producing an oscillatory

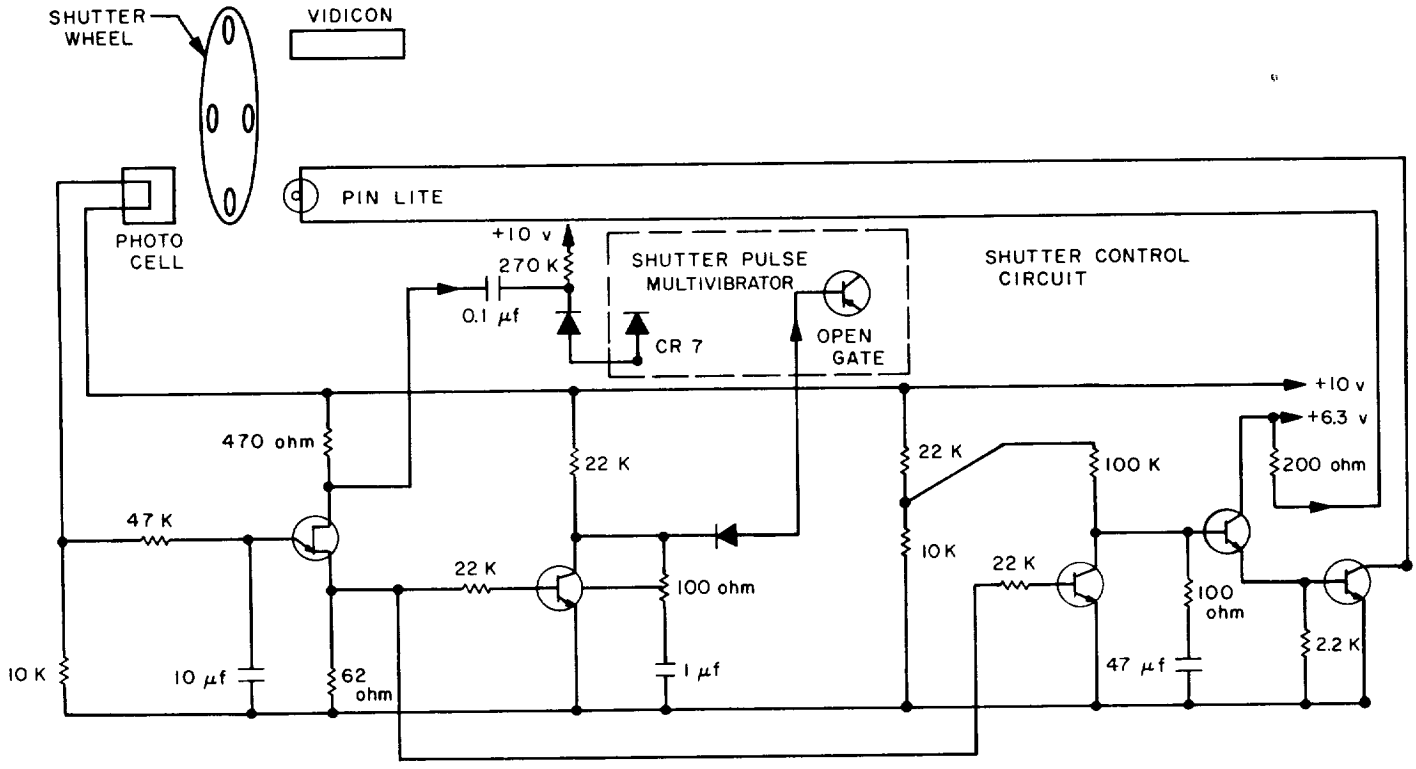

Fig. 20. Photo-cell control of open shutter

X. Space Instrument Systems

A. Magnetic Tape Study

1. Introduction

Magnetic tape as one of the four basic elements of a magnetic tape recorder is presently the subject of study to determine its relative suitability for various spacecraft data storage applications. It is certain that the selection of tape can significantly affect recorder performance. The goal of this study, therefore, is to ensure that particular selection which will result in optimal performance of the recorder in its specific application. It is also felt that such a study on a continuing basis will serve to provide up-to-date "state-of-the-art" information on magnetic tape products in general.

Dominant characteristics of a general nature are being examined with particular emphasis on the variations extant from brand to brand and among the various types of the same brand. Some of the more general characteristic variations known to exist in magnetic tapes are: wavelength sensitivity and signal-to-noise ratio, output uniformity, drop-out count, durability, erasability, tracking capability, and size with respect to a given storage capacity. The characteristics chosen for special scrutiny in this study are:

(1) Output amplitude and signal-to-noise ratio.

(2) Bit density capability.

(3) Uniformity of output and freedom from drop-outs.

(4) Physical durability.

2. Work Accomplished and Discussion

a. Summary. Most of the work accomplished to date concerns the first three items above. Electrical tests yielding signal amplitude and bit density data have been performed on various tapes, and the results plotted in a manner providing easy comparative evaluation. Photomicrographs of various coating surfaces have been made in order to gain some knowledge of present-day manufacturing capabilities, especially with regard to the probable incidence of tape-induced drop-outs. Additionally, some rudimentary work has been done in exposing tapes to high temperatures such as would be encountered in the present JPL sterilization procedures.

for each sweep, in order to give equal amplitude traces regardless of bit density.[2] The increasing variation in output from bit to bit as the density was increased is apparent. However, it appears that degradation in this respect was not serious until the step from 4280 to 8560 bits/in. was taken. This bears out what might be intuitively anticipated from examining the characteristic of Tape B in Fig. 1.

Fig. 3 also represents a continuous sequence of flux reversals at four different densities. However, in this oscillogram the sweep was increased considerably in order to illustrate longer term amplitude variations. A "drop-out" extending over approximately 150 bits can be seen on the maximum bit-density trace. This drop-out persists over a distance of about 15 mils on the tape. A particle of dust, loose oxide, or a sliver of backing material only a fraction of this length could have caused the "drop-out" by preventing the magnetic coating from achieving intimate head contact over this distance. Permanent defects in the coating can produce the same effect. Numerous tape coatings have been examined microscopically in an effort to judge their relative freedom from these "drop-out" inducing defects. Figs. 4, 5, and 6 are photomicrographs of typical defects found on various currently available instrumentation tapes.

Fig. 7 demonstrates the dependence of achievable bit density upon writing current amplitudes. Curve A is identical with Curve A as shown in Fig. 1. Curve X was made with the same tape but with the "write" current

[2]The actual levels can be determined from the output characteristic for Tape B in Fig. 1.

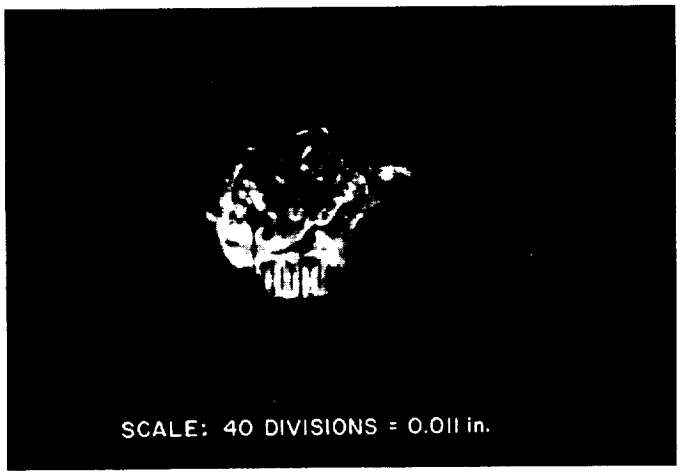

Fig. 4. A particle of backing (mylar) debris stuck to the oxide coating

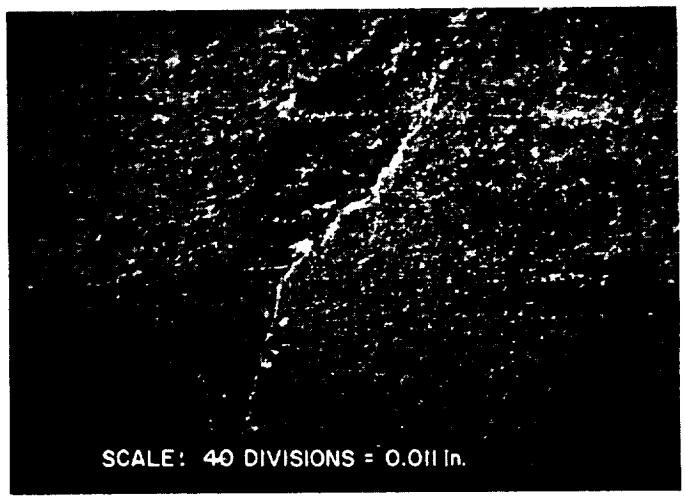

Fig. 5. A clump of binder material which appears to have been burnished or smoothed down

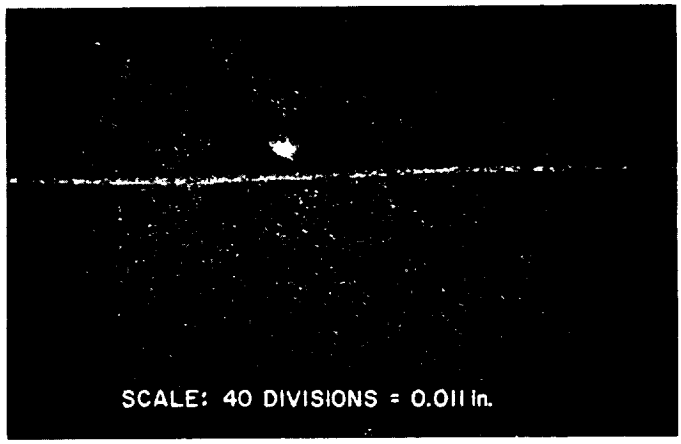

Fig. 6. A "hole" or declivity in the oxide coating

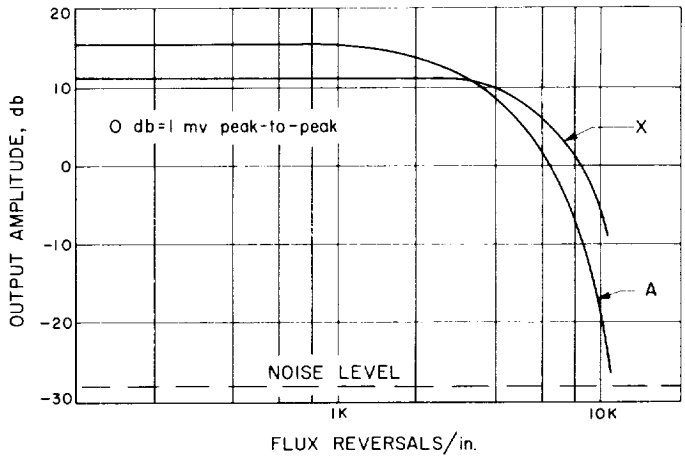

Fig. 7. Bit density dependence upon writing current amplitude

XI. Lunar and Planetary Studies

A. Evaluation of Electronic Filter Versus Nickel Filter for Cuk$_\beta$ X-Ray Discrimination

1. Introduction

X-rays emitted by the target in an X-ray tube are polychromatic; that is, they consist of radiation of several wavelengths. In X-ray diffraction analysis each of these wavelengths is capable of being diffracted according to the Bragg Equation $n\lambda = 2d \sin\theta$, where λ is the wavelength, d is the spacing between atomic planes in the sample from which diffraction occurs, θ is the angle at which incident X-rays strike the atomic planes, and n represents the order or harmonic of X-ray reflection. In order to decrease the number of superfluous diffraction peaks it is necessary to separate out the unneeded wavelengths of the X-ray spectrum. Standard techniques for achieving this are relatively inefficient and, when applied to limited-power goniometer-type X-ray diffraction systems such as the *Surveyor* lunar diffractometer, cause a serious loss of usable X-ray flux. Therefore, experiments have been conducted to review the existing methods of X-ray monochromatization and to evaluate which method is most efficient.

The spectrum from an X-ray tube consists of characteristic lines superimposed on a broad continuous band of radiation as shown in Fig. 1(a). The wavelengths of the lines are characteristic of the target element, which in the case discussed here is copper. The line spectra originate from the inner electron orbits of the target atoms, with several line series being produced depending on the energy level ($K, L, M, \cdots$) of the electron orbits. The K-series, which consist of two lines, k_α and k_β,[1] are most often the only ones used in X-ray diffraction because of the greater probability of K-series transitions. The k_β line is weaker in intensity ($k_\alpha/k_\beta = 100/22$) and has

[1]Actually, both k_α and k_β consist of several lines each; k_α is a doublet composed of two closely spaced lines in which k_{α_1}, the shorter wavelength, is about twice the intensity of k_{α_2}, and k_β consists of three closely spaced lines. It is difficult to resolve these finer lines and for most practical purposes k_α and k_β can be considered as single lines.

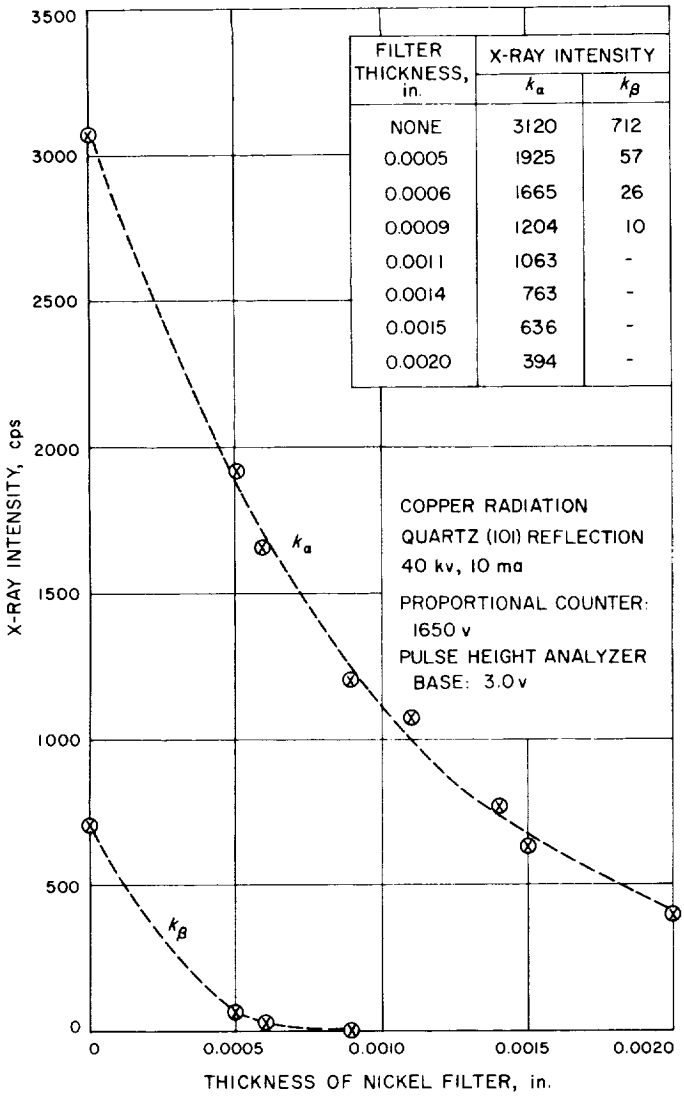

Fig. 2. Variation in absorption of the Cuk X-rays with change in nickel filter thickness

With conventional laboratory equipment, a 40% loss in k_α can be easily compensated for by increasing the power applied to the X-ray tube and thereby maintaining the desired k_α flux. In constant power instruments, however, such as the *Surveyor* X-ray diffractometer, desired k_α flux cannot be raised by this means, and the 40% loss of the working radiation is a critical concession.

4. Electronic Filter Method

Because the k_α and k_β radiations have different wavelengths, each will produce pulses of different energy in a proportional counter. Therefore, it is possible to employ pulse-amplitude discrimination (Ref. 2) to record only those pulses lying between specified energy limits.

The pulse energy resolution of presently available gas proportional counters is inherently limited (best values of about 14% W/A)[2] because of statistical fluctuations in the gas absorption and multiplication processes (Ref. 3). Therefore, because the wavelengths of k_α and k_β are relatively close to one another, the pulse energy distributions for k_α and k_β overlap (Fig. 3) and an electronic threshold designed to filter out k_β pulses also removes part of the k_α distribution. Thus, as with the nickel filter method, k_α intensity is reduced along with reduction of k_β.

The degree to which k_α is reduced by an electronic filter was determined experimentally using a Norelco pulse height analyzer (PHA) with adjustable baseline and window control with Cuk radiation. The intensity of a quartz (101) reflection for both k_α (26.6 deg) and k_β (24.3 deg) radiations was first determined using baseline and window settings which allowed the full distribution of pulse amplitudes to be employed. Then, with the goniometer set on the beta radiation of the (101) reflection (24.3 deg), the intensity of the beta peak was gradually reduced in increments to ¾, ½, ¼, ⅛, and 1/16 of its original value by decreasing the window setting (voltage) and thus gradually chopping off the higher voltage portion of the beta distribution. At each increment, the goniometer was moved up to the 2θ position of the alpha

[2] W is the pulse width at half height in volts and A is the mean pulse voltage.

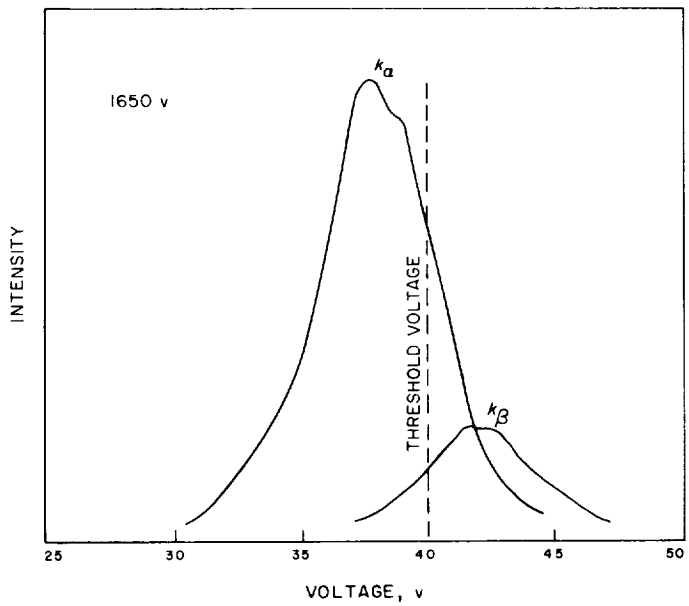

Fig. 3. Pulse distribution curves generated by Cuk radiation in proportional counter

In most applications, it is required that k_β be reduced by *more* than 80% of its original intensity. In this way, any k_β that is defracted will result in a peak on the diffraction pattern that is hardly distinguishable from random noise. In the case of the *Surveyor* diffractometer operating on the Moon, the average intensity of a diagnostic k_α peak will be about 800 cps (Fig. 6) and the average noise level n about 60 cps. For k_α peaks with intensity less than 800 cps, it is desirable not to see their related k_β peaks. Then, if the related k_β peak is to be indistinguishable from the noise, the ratio of k_α/k_β must be greater than $800/\frac{1}{2}n$ or $800/30 = 27$. Now, referring back to Fig. 5, we see that only the nickel filter method will allow a k_α/k_β ratio of 27 or greater. To achieve this value, k_β must be reduced by 89%, which requires the use of a nickel filter having a thickness of 0.0005 in. (Fig. 4).

Not only is the nickel filter most efficient but it is considerably more reliable due to its simplicity. Its successful operation depends only upon the proper choice of filter thickness and of wavelength of X-rays—two independent variables which, once chosen, are fixed and cannot vary. In contrast, the electronic filter method is highly dependent upon a relatively large number of dependent variables, which though fixed in principle, can vary considerably in practice; such as counter voltage, counter temperature, counter gas pressure, statistical fluctuation of ion-pair formation, electronic component temperature, etc. Instability in these parameters results in variations in the threshold level of the discriminator circuit, and a continually changing k_α/k_β ratio. Quantitative interpretation of peak intensity then is made extremely unreliable.

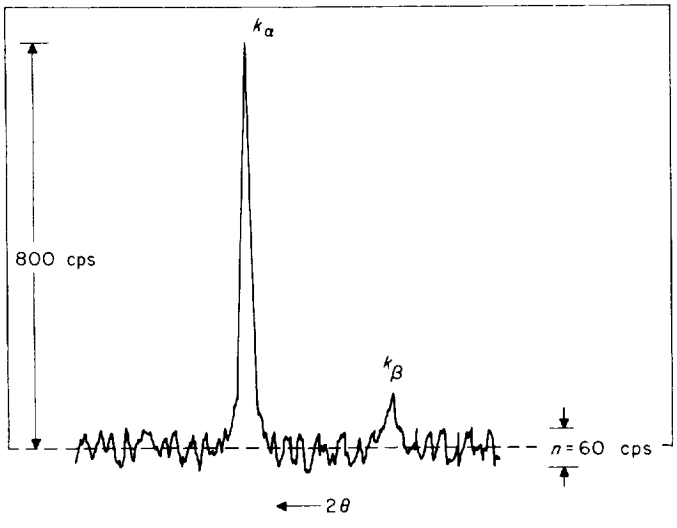

Fig. 6. Average peak and noise parameters for *Surveyor* X-ray diffractometer operating on Moon

On the other hand, the electronic filter method has the potential of being capable of completely eliminating k_β without degrading the k_α at all—if the resolution capability of proportional detectors can be improved, either by redesign of gas counters or utilization of new counters such as solid-state detectors. If this increased resolution could be achieved, a threshold window between the two pulses would completely separate them (Fig. 7). Furthermore, if standard gas counters could be operated at much higher potentials without gas discharge occurring, the k_α and k_β pulses would be separated by a greater voltage gap (Fig. 8), and therefore would be more easily isolated by a threshold voltage setting. This in turn would require greater voltage stability in the electronic system.

The ideal method of k_β discrimination might be to prevent the filling of electron vacancies in the K-shells of the target atoms by M-shell electrons and so suppress the excitation of the k_β line spectra.

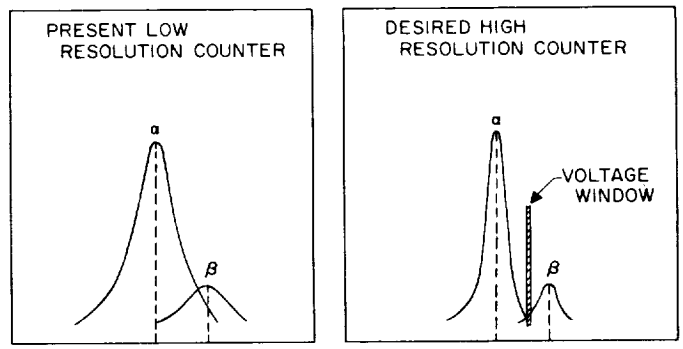

Fig. 7. Comparison of pulse distributions from low and high resolution counters

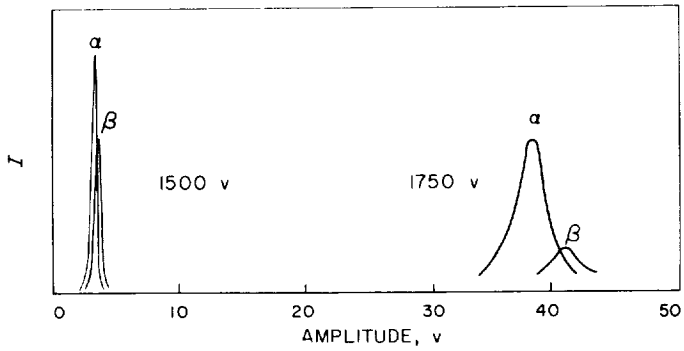

Fig. 8. Effect of counter voltage on pulse distributions